

University of Bologna

DEPARTMENT OF ELECTRICAL ENGINEERING
FACULTY OF ENGINEERING

Ph. D. in Electrical Engineering
XXI year
POWER ELECTRONICS, MACHINES AND DRIVES (ING-IND/32)

Design optimization and control strategies for PM Multiphase Tubular Linear Actuators

Ph. D. Thesis:

Filippo Milanesi

Tutor:

Prof. Giovanni Serra

Ph. D. Coordinator:

Prof. Francesco Negrini

Final Dissertation in 2009

To my parents and to Silvia

TABLE OF CONTENTS

| | |
|--------------------------|--------|
| TABLE OF CONTENTS | Page 9 |
|--------------------------|--------|

CHAPTER 1

Basic of Tubular Linear Machines

| | |
|--|---------|
| 1.1. Introduction..... | Page 11 |
| 1.2. Structure of linear actuators..... | Page 11 |
| A. Geometries..... | Page 11 |
| B. Forces and fundamental principle of operations..... | Page 12 |
| C. Applications..... | Page 13 |
| 1.3. Brief comparison among different linear actuators..... | Page 15 |
| A. Linear induction actuators..... | Page 15 |
| B. Linear permanent magnet synchronous actuators..... | Page 15 |
| C. Linear reluctance synchronous actuators..... | Page 16 |
| D. Linear switched reluctance and stepper actuators..... | Page 17 |
| 1.4. Technical characteristics of tubular linear drives..... | Page 17 |
| A. Linear tubular actuator..... | Page 17 |
| B. Linear tubular actuator competitors..... | Page 20 |
| 1.5. Iron core PM tubular linear actuator..... | Page 20 |
| A. Permanent magnets..... | Page 21 |
| B. Magnetic circuit..... | Page 22 |
| C. Windings..... | Page 25 |
| 1.6. Conclusions..... | Page 26 |

CHAPTER 2

Basic of Multiphase Drives

| | |
|--|---------|
| 2.1. Introduction..... | Page 27 |
| 2.2. Multiphase space vector representation..... | Page 27 |
| 2.3. Mathematical model of multiphase PM synchronous machines..... | Page 29 |
| 2.4. Main feature of multiphase drives..... | Page 30 |
| 2.5. Multiphase drives for torque capability enhancement..... | Page 31 |
| 2.6. Fault tolerant drives..... | Page 33 |
| 2.7. Multi-Motor drives..... | Page 34 |
| A. Multi-Motor drive concept..... | Page 37 |
| B. Machine connectivity..... | Page 39 |

| | |
|------------------------------|---------|
| C. Control..... | Page 41 |
| 2.8. Conclusion | Page 42 |

CHAPTER 3

Basic of Multiphase Drives

| | |
|--|---------|
| 3.1. Introduction | Page 43 |
| 3.2. Review of the design optimization methodologies | Page 43 |
| 3.3. Electromagnetic model | Page 44 |
| A. Preliminary design..... | Page 44 |
| B. Thrust force contributions..... | Page 44 |
| C. Fundamental hypothesis..... | Page 45 |
| D. Design of the magnets..... | Page 46 |
| E. Slider and stator design..... | Page 47 |
| F. Thrust force calculations..... | Page 48 |
| 3.4. Thermal model | Page 50 |
| 3.5. Mechanical model of the slider | Page 52 |
| A. Static equilibrium analysis..... | Page 52 |
| B. Maximum slider displacement..... | Page 55 |
| C. Reaction forces on the bearings..... | Page 56 |
| 3.6. Optimized design algorithm | Page 57 |
| A. Input parameter and design constraints..... | Page 57 |
| B. Preliminary design: solution procedure of the integrated model equations..... | Page 59 |
| C. Thermal model solution..... | Page 59 |
| D. Finite element analysis..... | Page 60 |
| E. Number of wires per slot optimization..... | Page 61 |
| 3.7. Conclusion | Page 63 |

CHAPTER 4

Optimized design of a PM tubular linear actuator and experimental results

| | |
|--|---------|
| 4.1. Introduction | Page 65 |
| 4.2. Definition of the design constraints | Page 65 |
| 4.3. Analysis of the influence of the air-gap length on the motor performance | Page 67 |
| 4.4. Optimized design of a tubular linear actuator | Page 69 |
| A. Preliminary design..... | Page 69 |
| B. FEM refining..... | Page 70 |
| C. Optimization of the number of wires per slot..... | Page 72 |
| 4.5. Experimental results | Page 74 |

| | |
|------------------------------|---------|
| A. Thrust force..... | Page 74 |
| B. Thermal behaviour..... | Page 77 |
| 4.6. Conclusion | Page 77 |

CHAPTER 5

Five-phase dual-motor series-connected drive: simulations and experimental results

| | |
|---|---------|
| 5.1. Introduction | Page 79 |
| 5.2. Description of the five-phase dual-motor seires-connected drive.. | Page 79 |
| A. Motor connections..... | Page 79 |
| B. Inverter voltage limit..... | Page 81 |
| C. Magnetic design of the five-phase tubular motor..... | Page 84 |
| D. Control scheme..... | Page 88 |
| E. Tuning of the regulators..... | Page 89 |
| 5.3. Experimental results | Page 90 |
| A. Start-up test..... | Page 91 |
| B. Position reference variation..... | Page 92 |
| C. Velocity variation..... | Page 92 |
| C. Independent contro test..... | Page 93 |
| 5.4. Conclusion | Page 93 |

| | |
|--------------------|---------|
| Conclusions | Page 95 |
|--------------------|---------|

| | |
|---------------------|---------|
| Bibliography | Page 97 |
|---------------------|---------|

CHAPTER

1

Basics of Tubular Linear Machines

1.1 Introduction

The demand for linear electric machine, specially for controlled motion, has registered a continuous growth in recent years, since its integration in industrial applications leads to important advantages [1]. Furthermore, the tubular structure seems to be attractive for industrial purposes due to both its closed form and the inherently absence of attractive force between the stator and the mover.

In this chapter the fundamental characteristics of the linear machines will be illustrated in order to highline their main advantages and drawbacks. Particular attention will be paid to the technologic developments in soft and hard magnetic materials, which enable the industrial realization of motor with high force density, improved dynamic behaviour within a relatively low cost.

Finally the attention will be focused on permanent magnet (PM) tubular linear motors.

1.2 Structure of linear actuators

A. Geometries

Linear electric actuators can drive payloads in a straight line providing thrust force directly, without any intermediate mechanical transmission such as gears, screws or crank shaft [2],[3].

The range of linear machine types available today corresponds almost exactly with the range of rotating counterpart [4], [5], [6], in fact It is known that cutting a rotating machine with a radial emi-plane and unrolling it, as depicted in Figure 1, a flat single-sided topology is obtained. If the rotating motor is cut by a radial plane and “squashed” as shown in Figure 2, a flat double-sided topology occur. Finally, the tubular linear topology is derived from the linear flat single-sided configuration rolling it up along the direction of motion, as depicted in Figure 3. These transformations turn the stator of the rotating machine into the primary of the linear machine, which is fed by a variable or fixed frequency supply, and the rotor into the secondary, which is equipped with permanent magnet, with a multiphase winding or it is

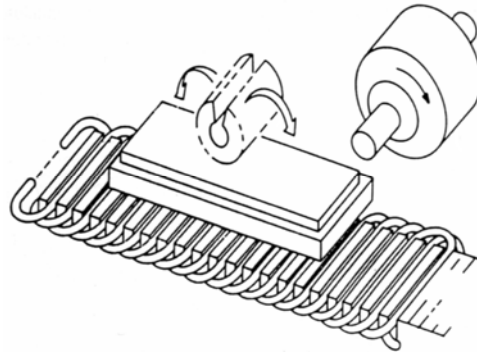


Figure 1-Imaginary process of splitting and unrolling a rotary machine to produce a single-side linear motor.

characterized by a variable reluctance ferromagnetic structure depending on the kind of the machine.

It is evident that, due to the finite length of the machine, linear or reciprocating motions are achievable only by an extension of the linear stator or of the linear rotor. The result, shown in Figure 4, is the so called long stator or short stator machine. In practical applications both of them are used depending on the appliance requirements, for example, short stator solutions are often used in packaging and manufacturing sectors, while long stator types are adopted for transportation systems. The moving part of the linear machine is often called forcer, mover or slider and can coincide both with the primary or with the secondary of the machine.

B. Forces and fundamental principle of operations

In classical rotary machines there are two forces acting on the rotor surface [7]: a tangential force which produces the torque and a radial force, acting perpendicularly to the rotor surface. This latter force sums to zero around the circumference due to the cylindrical

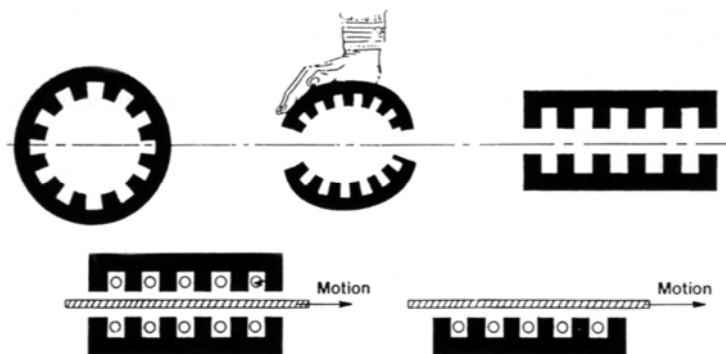


Figure 2-Imaginary process of cutting and squashing a rotary machine to produce a double-side linear motor.

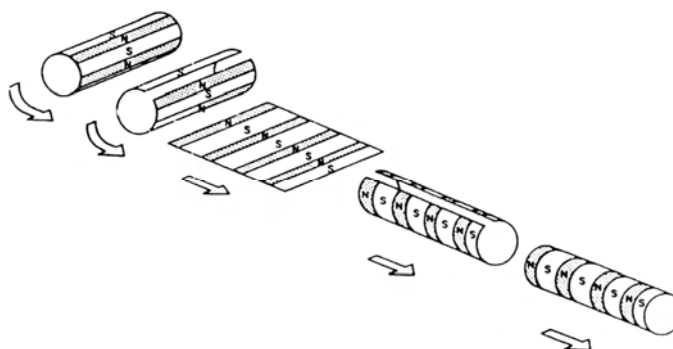


Figure 3-Conceptual transformations to obtain a tubular motor starting to a rotary machine, passing through a flat linear actuator.

symmetry of the machine. When the machine is “transformed” to create a linear machine, the tangential forces sum each other to constitute the driving force. The normal forces in flat configurations are not now balanced and a large net force acts between the unrolled rotor and stator. The ratio between the latter and the thrust force is worthy of considerations, typical value vary in the range $8\div 10$. The propulsion force on the moving part of a linear actuator is generated in different ways, according to the machine’s operation principle:

- linear induction motors produce thrust force by the electromagnetic interaction between the primary translating magnetic field, generated by an alternate current multiphase winding, and the induced current on the multiphase winding or on the bar of the secondary;
- linear stepping or switched reluctance motors create thrust force by the action of a magnetic field, produced by electronically switched direct current windings, and an array of ferromagnetic poles or a variable reluctance ferromagnetic rail;
- linear synchronous motors produce thrust by the action of travelling magnetic field, produced by an alternating current multiphase winding, and an array of magnetic poles or a variable reluctance ferromagnetic rail;

The aforementioned list suggests structural differences among the range of linear machine types; in this way the presence/absence of windings in the primary and in the secondary, the use of permanent magnets, the utilization of innovative materials determine the specific linear motor characteristics.

C. Applications

The use of linear actuators has received a growing interest in several applications [8], [9], since a large number of linear or reciprocating motions is required.

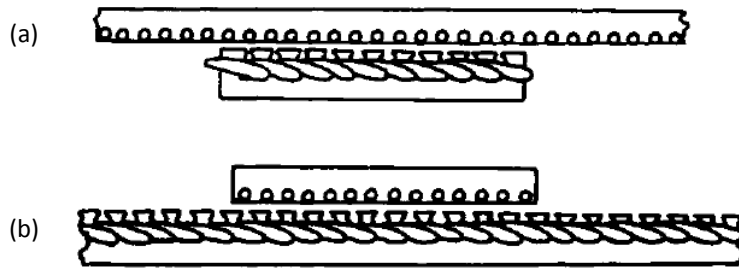


Figure 4-Linear motor with the so called short stator (a) or long stator (b).

Linear machines show performances comparable with the ones of the rotating counterpart; developments in materials, design methodologies and in manufacture technologies have increased force density, dynamic behaviour, robustness and reliability. In some applications the design constraint limits or reduce performances of linear motors, viz. in transport sector where large air-gap are obliged, but these restrictions are more than compensated by many characteristics of linear motors that cannot be achieved by rotary equivalents.

Historically the first linear motor topology that took place in industrial and transport applications was the induction one, but in the last 25 years the improvements in power electronics and permanent magnet materials has driven the linear synchronous machine toward increasing number of utilizations.

Nowadays flat and tubular linear motors are applied for controlled motions and servo actuation in high-speed packaging and pick-and-place machines, in automated structure such as industrial robots [10], fast manipulators and automatic machine tool feeder [11]. Other applications are reciprocating compressors and refrigerators [12]. The aforementioned applications share relatively low power requirement and they constitute the main commercial demand of linear drives, furthermore they are often customized solutions.

High-medium power applications are less frequent, however research are being carried out in this particular field. Linear drives have been proposed in energy production systems, free-piston energy converter was studied in [13] while tidal and wave-energy conversion systems were analyzed in [14], [15].

An important application field concerns with transportation systems for public and factories [16]; linear 'people-movers' are currently used in operations at several international airports, while magnetically levitated or wheels supported trains are used in Japan [1] and Europe.

Linear motor drives are strong candidates for both low-speed and high-speed mass transit applications. Systems using linear induction and synchronous machines are prevalent in industry.

The future prospects of application of linear drives are expected to involve not only traditional sectors, such as transport, material processing and automation equipments, but also new one, like in aerospace and automotive sectors.

1.3 Brief comparison among different linear actuators

Researches and studies have been carried out for all type of linear machines, but only some of them have been focused for real applications. The feasibility, the cost effectiveness, the robustness and the reliability are key aspects that must be owned by an industrial product. For some kind of motors most of these properties are inherently satisfied but for other motor types these requirements have been satisfied with the developments of materials and of digital controllers.

The latters covered an important role for the industrial diffusion of linear actuators. In fact, control strategies for direct drive systems and servo actuations have become more complex and precise, capable to generate smooth motion even in hard dynamic operations.

The operational principle strongly affects the motor structure, thus it determines their attitude to be used for specific applications.

A. Linear induction actuators

Linear induction actuators (LIAs) have been built with an a.c. multiphase winding in the primary, whilst the secondary houses a cage or a short-circuited three phase winding. However, conventional secondary configurations have a conducting plate on a solid iron plate or may have only the former [4], [17]. The plate solution gives an easy-manufactured machine, with a robust and relatively cheap secondary, suited for hostile environment or for low maintenance applications. The core of primary and secondary of flat LIAs, except for the plate secondary solution, is laminated in order to reduce core losses and magnetizing current, furthermore open-slot or semi-closed slot geometry facilitate their construction. For tubular structure, open slot geometry has been used since recent developments of soft magnetic materials, viz. soft magnetic composites. In fact, laminations of tubular core with standard technologies manifest problems for flux paths or for construction feasibility.

The LIAs configuration depend on the travel length: for short travel applications, viz. 0.5 m, the tubular structure is favourite whilst for travel length up to 2÷3 m the moving primary flat configuration is preferred, and a flexible cable supplies the windings. For greater travel length long primary flat configurations are used; the primary sections are placed along the track and the secondary acts as the mover, the former are turned on only when the latter is in their proximity.

B. Linear permanent magnet synchronous actuators

Linear permanent magnet synchronous actuators (LPMSAs) has penetrated into the market and established the practical application, since developments in hard and soft

magnetic material occurred [16]. Progress of high-energy rare-earth magnets, whose remanence can be up to 1.2 T at 20°C and whose operating temperature can be up to 150°C, has permitted to reach proper performances for several direct-drive applications. There is no doubt that permanent magnet machines are more expensive than induction machines. However, they offer improved performance especially in terms of force density and dynamic response. This is particularly true in small sizes actuators, where the magnetising current for induction machines becomes important to the disadvantage of the thrust force. Unfortunately, the presence of magnets can be a problem in polluted environment due to stray magnet fields, particularly in presence of iron particles, since they can be attracted and cause a machine fault.

Primary core structure for flat and tubular LPMSAs is similar to the primary of LIAs. The LPMSAs secondary is made up of permanent magnets, used for excitation flux production, and a laminated core. Magnets can be buried in the core structure or can be surface mounted.

Moving primary flat LPMSAs are used for travel up to about 3 m, whilst for longer travel moving magnets flat configurations are used. For travel length of less than 1 m tubular configurations may be preferred, since tubular structures make better use of materials, resulting in compact actuators.

C. Linear reluctance synchronous actuators

Linear reluctance synchronous actuators (LSRAs) have the same primary characteristic of LIAs and LPMSAs, but the secondary does not house windings or PMs. The thrust force production is entrusted to the interaction between the secondary magnetic circuit anisotropy and the primary travelling magnetic field. These actuators are specifically designed to emphasize the magnetic anisotropy between q-d axes, in fact the force production is proportional to the secondary saliency. Recent research in rotating reluctance machine has led to development also in the linear counterpart, resulting in a relatively inexpensive motor with good performance indices.

Good energy conversion is achieved by thin air-gap, but this feature implies large normal forces, viz. large attractive force between the stator and the mover. Thus the mechanical part of flat configuration merits special treatment, in order to obtain a sufficient reliability and robustness.

LSRAs can constitute an alternative to LPMSAs and LIAs. Compared with the formers, they have lower costs and can operate at very high speed because of the easier field weakening capability and the rugged rotor. It doesn't have secondary winding that travels at synchronous speed, so the controller is simpler than other of AC machines. If compared to LIAs, it has theoretically no secondary losses and a comparable force density depending on the design of the motors.

In conclusion, LRSA are a rarity in industrial drives, although they are not completely unknown [18], [19].

D. Linear switched reluctance and stepper actuators

Linear switched reluctance motor (LSRM) is an electric machine which possesses simple structure with a winding only on the stator. The costs are lower than other motors due to its simple construction [20].

Further, the windings are concentrated rather than distributed, making them ideal for low-cost manufacturing and maintenance. Concentrated windings enable a naturally fail-safe system that can operate even with a phase shorted or open [21]. The availability of numerous low cost converter topologies to drive them makes the LSRA advantageous over linear induction and permanent-magnet synchronous motors, which incur a higher cost and have thermal drawbacks [22], [23]. Although LSRA have plenty of advantages, the fact that the force ripple deteriorates the performance restricts its application to precision devices. Much research has been reported to reduce force ripple, and improved performances have been enhanced [24], [25]. Tubular construction of this kind of motor permits to overcome the attraction force between excitation and mover, since the axial symmetry of the machine allows an inherent neutralization of this force [26].

In linear stepper actuators (LSAs) the motion is caused by the tangential force which tends to align poles of the moving part with the excitation poles of the static part [27], [28]. In contrast to rotary counterpart, where the normal force of attraction between stator and rotor pole faces is neutralized by the same force acting between the diametrically opposite pair of stator and rotor poles, the normal force in the linear counterpart is high and can be a serious mechanical problem. The problem may, to some extent, be overcome by the use of a symmetrical doubly-sided version of the rectilinear counterpart.

1.4 Technical characteristics of tubular linear drives

Tubular linear drive offers several advantages in comparison with both the flat linear and the rotary counterpart. Some benefits are inherently introduced by the tubular structure of the motor, hence they belong only to this category of motor, whereas other advantages are commonly present in the other linear machines.

A. Linear tubular actuator

Tubular linear actuator is obtained through the transformation depicted in Figure 3, which awards special features to the motor if compared to the rotating counterpart. The first one concerns the motor windings, indeed they do not have the end-windings, thus all the conductors and the phase current actively participate to the magnetic field production [6]. The end-winding Joule losses disappear, hence an increased coil efficiency and a better power-to-weight ratio compared to both the flat and the rotating topology results. The

winding shape looks like a ring of conductors, so it is easy to implement and it is suited to be industrially produced. Furthermore, the tubular geometry arises with inherent feature of self neutralization of normal forces acting between the stator and the mover, since they are symmetrically distributed over the mover circumference. The piston-like appearance of the tubular linear machine gives the designer a firm foothold to connect the mechanical load, and the closed frame makes it capable to operate in polluted and hostile environments [29]. On the other hand, the tubular topology imposes limits in the maximum mover stroke, since excessive mover blending may cause vibrations and mechanical damage of the motor.

Among the various linear actuators, tubular topologies with permanent magnet excitation are particularly attractive, since they do not show the typical assembly problems of linear open machines, having indeed a compact structure and a high force density [30]-[31], [32]. Unfortunately, the permanent magnets interact with stator core determining a disturbance force, which can cause negative effects such as vibrations, noises, positioning errors and non-uniform movement at low speed. Such a force in linear actuators is the sum of two components: the cogging force and the extremity force [33]. The former is generated by the tendency of the magnets to align with the stator at positions where the permeance of the magnetic circuit is maximized and has a spatial wavelength depending on the pole number, the slot number and the pole-pitch, whereas the latter depends on the interactions between the finite length of the armature core and the moving magnet, and has a spatial wavelengths of one pole-pitch. The effects of disturbance force can be minimized at the motor design stage [34], [35], employing methods such as skewing and optimally disposing the magnets, and optimizing the length of the armature core [36]. Further improvements to get smooth motion can be obtained by employing a current-shaping control strategy [37].

The production of thrust force makes all linear drives suited to simplifying the mechanics in automated machine through direct-drive actuators, jointly to the adoption of advanced control methodologies.

To achieve precise motion control, most of these machines use rotary electrical motors as their prime motion actuators, and couple their output shafts to mechanical motion transmissions as reduction gear, belt, ball screw, pinion-rack, etc. Though this is the most widely used method, mechanical transmissions suffer of several drawbacks, which are emphasized through the high-dynamic performances of modern PM drives and controls.

The use of mechanical transmissions increase the whole dimensions of machines and their costs. Figure 5 shows some applications where the linear drives can replace the rotating counterparts.

The most evident disadvantages of indirect drives are:

- dead points in mechanical chain that can cause problem for position control.
- backlashes, which decrease the machine precision particularly during the inversion of the motion.

- stiffness
- torsional elasticity and bending of the shafts, imputable of resonance which represents in many cases an insuperable limit both for the accuracy of the positioning control and for the maximum speed.
- additional frictions which cause power losses, hence reduced efficiency.
- additional mechanical parts reduce the system reliability.

All these aspects engrave negatively on the performance of the system in terms of accuracy, resolution and repeatability. Applications with short stroke enlarge these limits, since the reduction of the positioning times increase the accelerations, viz. the dynamic aspects.

The direct-drive philosophy, which provide thrust force directly to a payload, offer numerous advantages over their rotary-to-linear counterparts. All the previous drawbacks are overcame, since the mechanical transmission is now eliminated. Linear motors become an integral part of the automatic machines, which are capable of higher dynamic

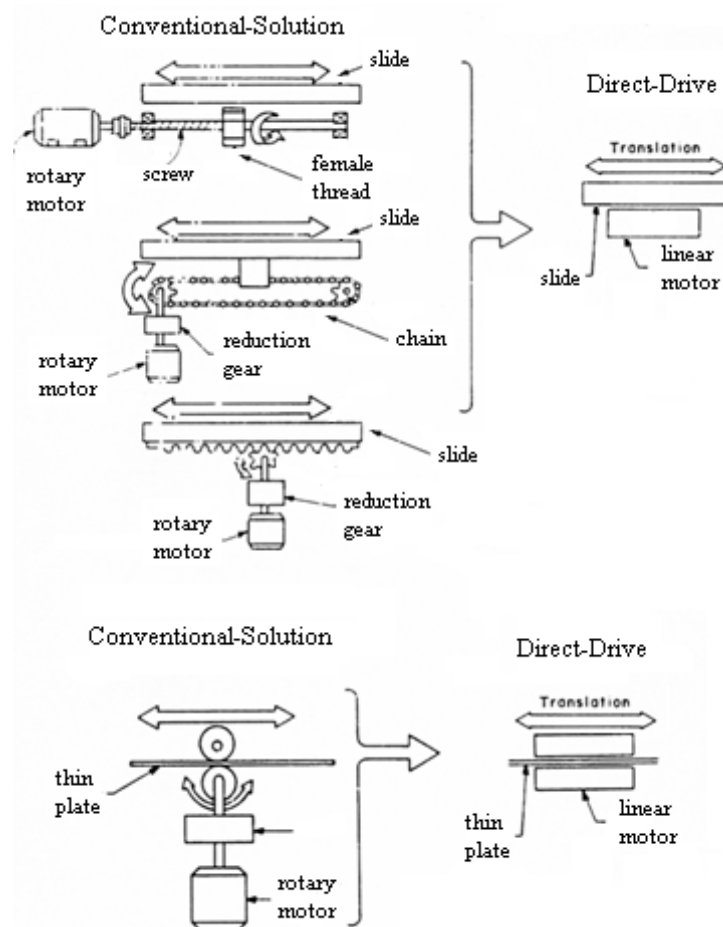


Figure 5-Example of some applications where the linear drives can replace the rotating counterpart.

performance, improved reliability and higher control bandwidth than the traditional machines.

B. Linear tubular actuator competitors

Pneumatic and hydraulic pistons have the same appearance of tubular electric actuators, thus they constitute an alternative choice to the electric counterpart.

Industrial applications often require controlled motion and, in some cases, also controlled force. Traditional hydraulic and pneumatic thrusters often use open-loop force control. The force is created by applying pressure to a working gas or fluid in a hydraulic or pneumatic cylinder. A piston then converts the pressure to a force applied to the load.

This solution shows several disadvantages if compared with tubular linear electric one, first of all, an electric tubular drive has larger accuracy, readiness and control reliability, it is free-maintenance and it has easier energy supply availability, and secondly an electric drive does not present any fluid dripping.

1.5 Iron core PM tubular linear actuator

Among the various linear actuators, tubular topologies with permanent magnet excitation are particularly attractive, since they do not show the typical assembly problems of linear open machines, having indeed a compact structure and a high force density. Figure 6 depicts a simplified three-dimensional sight of a PM tubular motor with axially magnetized magnets.

Up to few years ago the tubular motor was not used in industry because of constructive and performances reasons. Ironless actuators exhibited low specific force since high-energy rare-earth magnets had been developed, while iron-core motors had the realization problem of a magnetic circuit suited for the flux line path.

Usually, in the traditional rotating motors the planar lamination of the magnetic core

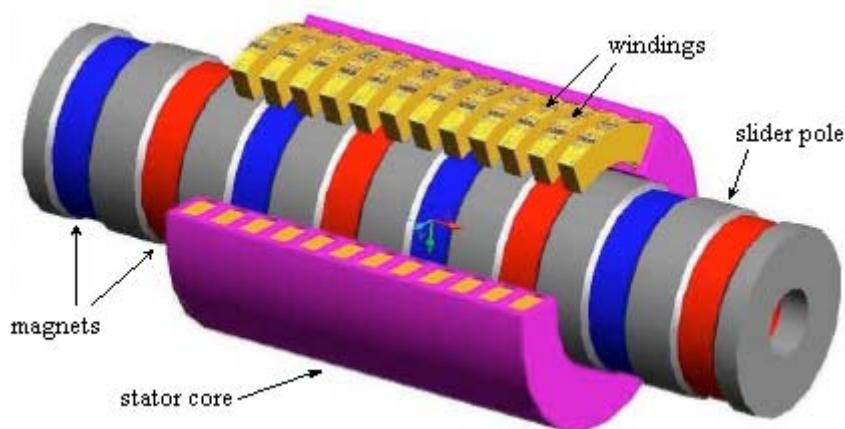


Figure 6-Three-dimensional sight of a PM tubular motor with axially magnetized magnets.

interrupts the circulation of eddy current induced by time-variable magnetic fields. In a tubular motor eddy currents flow around the actuator circumference, hence their interruption should be realized with “pie-slice” lamination [38], as shown in Figure 7. The latter is practically unfeasible, thus other solution were adopted. Core lamination able to shorten the paths of the induced current can be longitudinal or transverse with respect of the direction of motion [5], [6]. Both of them show drawbacks: the former exhibits the practical difficulty to precisely align the laminations of every core all around the motion axle, as shown in Figure 8, while the latter determines an increase of the magnetic circuit reluctance due to the substantial total thickness of the insulations among the laminations on the motor back-iron which has to be crossed by the flux lines. These problems have been overcome thanks to the scientific and industrial development, which has produced the Soft Magnetic Composites (SMC). This class of materials is basically that of iron powder particles coated with an electrically insulated layer as shown schematically in Figure 9. These powders can be compacted in complex form and, after a thermal treatment, are ready to use showing isotropic magnetic properties.

Finally, windings of this kind of motor have not frontal connections, resulting in a compact structure and a great density of force.

The principal parts that form a PM tubular linear actuator will be shortly described in the following sections.

A. Permanent magnets

Permanent magnet tubular actuators can be constructed with surface-mounted radially magnetized magnets, depicted in Figure 10, or with axially magnetized magnets, shown in Figure 11. An interesting comparison between the two solutions was carried out in [39], where it is concluded that the axially magnetized machine has a higher force density, but more permanent magnet material is required. If the same volume of permanent magnet is used, the two topologies lead to the same force density. However, axially magnetized machine should be preferred because axially anisotropic rare-earth magnets are usually less

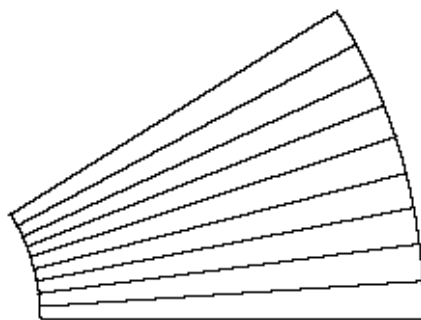


Figure 7-conceptual “pie-slice” lamination for magnetic core of tubular actuator.

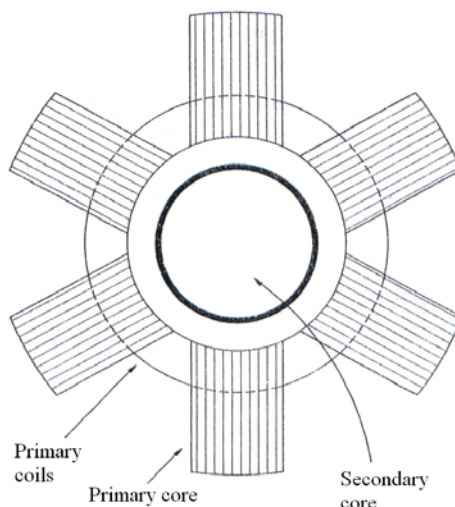


Figure 8-Practical arrangement of stator core using longitudinal laminates with respect of the direction of motion.

expensive and widely available.

Magnet typology for this actuators have to be selected considering the motor performance target fixed in design stage. However, the most diffused magnets are in Ferrite or in Nd-Fe-B. The first ones represent the most economic choice, having low remanence, low-energy product and a strong temperature de-rating.

The Nd-Fe-B magnets have at present the most elevated specific energy, similar consideration concerns the remanence value and the intrinsic coercive field, even with magnet temperature of 100-150°C. Typical value of main parameter for Ferrite and Nd-Fe-B magnet are summarized in Table I.

All of these elements have to be considered during the motor design to make sure that the magnet doesn't suffer permanent damages that jeopardize the reliability and the performances of the motor.

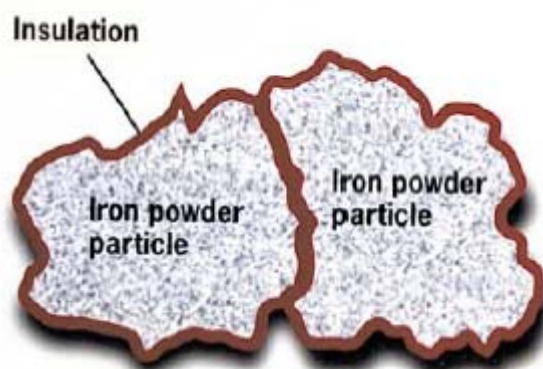


Figure 9-Schematic picture of SMC material.

Table I-Comparison among main parameter of ferrite and Nd-Fe-B magnets.

| Parameter | Ferrite | Nd-Fe-B |
|-------------------------------------|-------------|-------------|
| Br [T] | 0.2÷0.5 | 1.1÷1.3 |
| Hc [kA/m] | 150÷295 | 700÷1000 |
| Relative recoil permeability | 1.1 | 1.08 |
| Temperature coefficient of Br [%°C] | -0.11/-0.12 | -0.54/-0.60 |
| Temperature coefficient of Hc [%°C] | -0.2 | +0.3 |

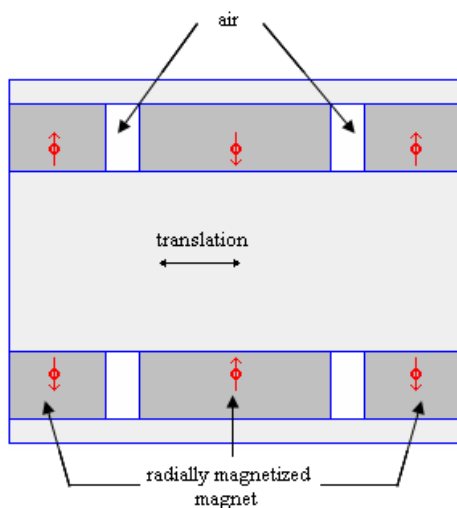


Figure 10-Axial section of a tubular mover composed of radially magnetized magnets.

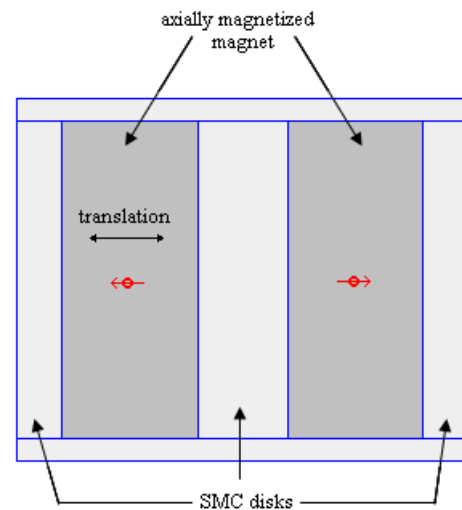


Figure 11-Axial section of a tubular mover composed of axially magnetized magnets.

B. Magnetic circuit

The use of SMC material allows to overcome the problem of a proper magnetic circuit for tubular actuators, since flux paths have both radial and axial direction. Magnetic

properties of such a material have to be analyzed in order to fully understand its potentiality [40].

In general, SMCs have lower initial permeability, lower saturation induction and higher iron losses at 50-60 Hz than the laminated steel. These limitations can be cancelled if the isotropic 3D behaviour of SMC will be exploited [41], [42]. Further, the aforementioned characteristics are strongly dependant on the kind of powder and on the transformation process used to obtain the finished component. In particular, the electromagnetic and mechanical properties will depend on the added lubricant/binder and on the process, for example, cold or warm compaction.

A low amount of additive results in a powder mix that can be compacted to higher densities and heat treated with higher temperature, which is beneficial for the magnetic properties, as shown in Figure 12. During compaction stress is introduced in the particles, which deteriorates the soft magnetic properties. The higher the heat-treatment temperature is set, the higher the degree of stress relief. However, it is crucial that no sintering take place

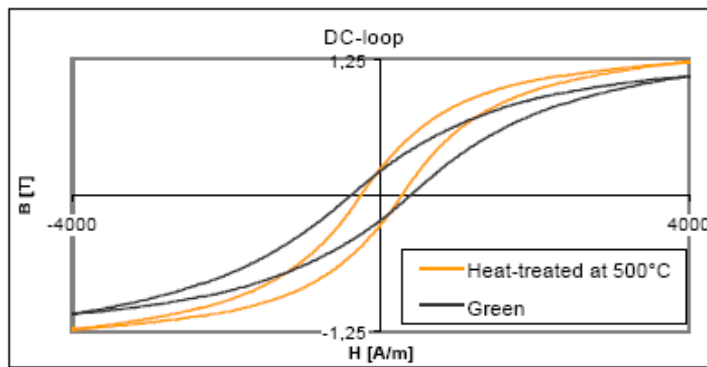


Figure 12-Heat-treatment effect in hysteresis-loop characteristic of Somaloy 500®.

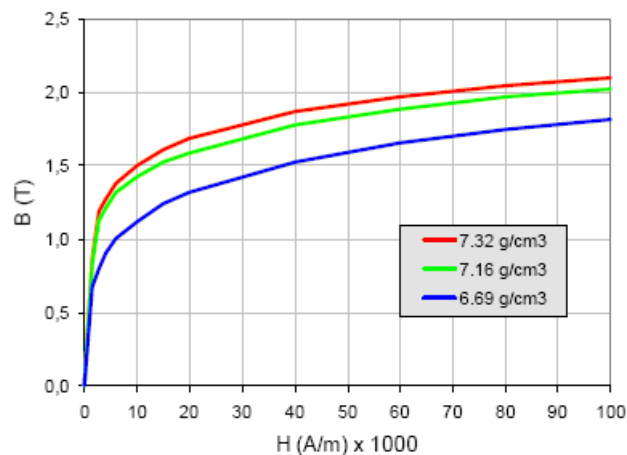


Figure 13-Effect of material density on B-H curves of Somaloy 500®.

between the particles, as the dynamic losses would increase rapidly with frequency.

As presented in Figure 12, the magnetic induction depends heavily on the compaction pressure of the material, because it determines the material density. A higher magnetic induction for a certain applied field means improved performance of the motor. Compared to laminations, SMC has normally a slightly lower induction level, though the difference is small at higher fields. Hysteresis losses are worse if compared to that one of laminations, instead dynamic behaviour is better due to reduced eddy current losses. This means that at a certain critical frequency, typically around a couple of 100 Hz, the losses will be lower in the SMC-material than in laminations. The maximum relative permeability is significantly lower in SMCs compared to the in-plane property of steel laminations.

One of the main advantage with SMC is its 3D-properties; the material is isotropic, thus magnetic flux can flow equally well in all directions. Another advantage is the opportunity to obtain 3D-shapes by a compaction process. The combination of these two features applied to particular machines, such as the PM tubular one, can compensate the lower magnetic properties than laminations. Tubular PM machines have high natural reluctance due to presence of magnets, thus the permeability is of less importance and good performance can be still achieved.

The influence of the choice of SMCs on the performance of tubular permanent magnet machines was carried out in [43], where it is shown that SMC machines have a slightly inferior performance if compared with laminated one, but they are easier to manufacture, and, therefore, potentially be lower cost.

C. Windings

The primary winding of tubular motors has simple disk-shape, like that one depicted in Figure 14. The tubular motor, for its own nature, has a very simple statoric structure, thus its construction consists only in an alternatively stack of SMC disks and windings.

The winding can be pre-assembled and pre-compacted in order to obtain good slot filling coefficient.

The benefits arose by this operation are manifold: the electric exploitation of the slot is increased, and finally the thermal exchange of winding is improved, bringing to a more uniform distribution of the winding temperature.



Figure 14-Disk-shaped stator windings of tubular linear actuator.

1.6 Conclusion

An overall comparison among different topologies of linear machines has been well developed, showing merits and demerits of each type of motor. Hence, it results that, among the various linear actuators, tubular topologies with permanent magnets are particularly attractive. In fact they do not show the typical assembly problems of linear open machines, then they have a compact structure, moreover soft and hard magnetic material development bring them to higher force density. These machines have excellent characteristics as servo motor, which make them suited to the use in automated industrial machines.

CHAPTER 2

Basics of Multiphase Drives

2.1 Introduction

The conventional structure for variable-speed drives consists of a three-phase motor supplied by a three-phase voltage source inverter (VSI). The converter can be viewed as a decoupling interface between the three-phase mains and the motor. Thus, the need for a specific number of phases, such as three, disappears. Furthermore, the development of power electronics makes it possible to consider the number of phases as an additional design variable.

Nowadays, there is an increasing attention towards multiphase drives. Indeed they offer a greater number of degrees of freedom compared with three-phase motor drives, which can be utilized to improve the drive performance [44], [45]. In this chapter the fundamental aspects of multiphase drives will be presented, focusing the attention to the so called multi-motor multiphase drive.

2.2 Multiple space vector representation

As known, a multiphase motor drive cannot be analyzed using the space vector representation in a single d-q plane. It is known that, to completely describe a multiphase electromagnetic system, the space vector representation in multiple d-q planes (multiple space vectors) must be adopted [46]. Some modern approach to the modulation of multiphase inverters have overcome the inherent difficulty of synthesizing more than one independent space vector simultaneously in different d-q planes, in order to fully exploit the potential multiphase motor drives [47]. They have shown that the multiple space vector notation is well suited to represent and to analyze multiphase systems.

In a n-phase system, for a given set of n real variables $x_1, x_2, x_3, \dots, x_n$, a new set of variables can be obtained by means of the following symmetrical linear transformations [48]:

$$\bar{x}_h = \frac{1}{n} \sum_{k=1}^n x_k \bar{\alpha}^{h(k-1)}, \quad (h = 0, 1, 2, \dots, n-1) \quad (2.1)$$

where $\bar{\alpha} = \exp(j 2\pi / n)$.

With the exception for $h = 0$ (and $h = n/2$ for even number of phases), the quantity \bar{x}_h is a complex number and it is called space vector component of sequence h , or space vector on the $(d-q)_h$ plane.

It can be shown that the space vector component of sequence h is related to the space vector component of sequence $n - h$ through a complex conjugate relationship, furthermore the space vector component of sequence $n - h$ coincide with the space vector component of sequence $-h$. These properties can be synthesized by the following equation:

$$\bar{x}_h = \bar{x}_{-h}^* \quad (2.2)$$

The real variable $\bar{x}_0 = x_0$ is obtained for $h = 0$ and is called zero-sequence component, whereas the additional real space vector component of sequence $n/2$ appears for an even number of phases only.

Using the aforementioned classifications and applying (2.2), the space vector transformations can be rewritten as follows:

$$\bar{x}_h = \frac{2}{n} \sum_{k=1}^n x_k \bar{\alpha}^{h(k-1)} \quad (h = 1, 2, \dots, r) \quad (2.3)$$

$$\bar{x}_0 = \frac{1}{n} \sum_{k=1}^n x_k \quad (2.4)$$

$$\bar{x}_{n/2} = \frac{1}{n} \sum_{k=1}^n x_k (-1)^{k-1} \quad (2.5)$$

where $r = n/2 - 1$ for an even phase number and $r = (n-1)/2$ for an odd phase number. The corresponding inverse transformations are:

$$x_k = \bar{x}_0 + \left(\bar{x}_{n/2} (-1)^{k-1} \right) + \sum_{h=1}^r \bar{x}_h \cdot \bar{\alpha}^{h(k-1)} \quad (k = 1, 2, \dots, n) \quad (2.6)$$

where the symbol “.” represents the dot product.

In the particular case of balanced and sinusoidal operating conditions (sequence 1), the space vector \bar{x}_1 assumes a special relevance being the only space vector different from zero.

However, it is opportune to emphasize that, in the general case, all the r space vectors as well as the zero-sequence component are necessary to completely describe the n -phase system.

2.3 Mathematical model of multiphase PM synchronous machines

The behaviour of the rotating n -phase synchronous machine with surface mounted PM can be described in terms of multiple space vectors by the following equations written in the stator reference frame:

$$\bar{v}_{sh} = R_s \bar{i}_{sh} + \frac{d\bar{\varphi}_{sh}}{dt} \quad (2.7)$$

$$\bar{\varphi}_{sh} = L_{sh} \bar{i}_{sh} + M_{se,h} i_e e^{jh\theta} \quad (2.8)$$

$$v_e e^{j\theta} = R_e i_e e^{j\theta} + \frac{d}{dt} [\varphi_e e^{j\theta}] \quad (2.9)$$

$$\varphi_e e^{j\theta} = L_e i_e e^{j\theta} + \frac{n}{2} \sum_{h=1}^r M_{se,h} \Re[\bar{i}_{sh}] \quad (2.10)$$

From the magnetic coenergy, the torque equation can be obtained as follow:

$$T = \frac{n}{2} p \sum_{h=1}^r h M_{se,h} (\bar{i}_{sh} \cdot j i_e e^{jh\theta}) \quad (2.11)$$

where p is the pole pairs number, h is the multiple space vector index, and ϑ is the electrical position of the rotor reference frame.

Multiphase drives enable the independent control of a series of multiphase motors supplied by one multiphase inverter, provided that the machines are designed to produce sinusoidal-field distribution in their air-gap. The latter feature simplifies the torque expression (2.11), in fact in this case only the first current space vector influences the torque production. Moreover, considering a PM brushless tubular linear actuator, the equations (2.7)-(2.10) remain unchanged, whereas equation (2.11) becomes the expression of the thrust force (2.12) under the assumption of negligible end-effects.

$$F = \frac{n}{2} \frac{\pi}{\tau_p} M_{se,1}^t (\bar{i}_{s1} \cdot j i_e e^{j\theta}) \quad (2.12)$$

where τ_p is the pole pitch, $M_{se,1}^t i_e$ is the voltage constant expressed in $V/(m/s)$ and the relation between electric position \mathcal{G} and linear position x is:

$$\mathcal{G} = \frac{\pi}{\tau_p} x \quad (2.13)$$

2.4 Main feature of multiphase drives

Multiphase variable speed drive has received growing interest since the second half of the 1990s. The area of electric ship propulsion and their developments acted in that period as propeller for the research [49], [50]. Nevertheless, oldest records concerning this topic dates back to the second half of the 1960s. Historical technical reasons that urged to adopt the multiphase drive solution instead of three-phase one are listed below [51]:

- 1) Multiphase variable speed drive reduces the stator current per phase, for a given motor output power.
- 2) The use of more than three phases offer an improved reliability due to the fault tolerance features of multiphase drives
- 3) Multiphase machines present reduced pulsating toques produced by time-harmonic components in the excitation waveform.

As stated at point n°1, the use of multiphase drive instead of the three-phase one helped to overcome the problems related to high-power applications with current limited devices. For a given motor power, an increase in phase number determines a reduction in power per phase, enabling the use of smaller power electronic devices in each inverter leg, without increasing the voltage per phase [52]. This is still a solution adopted for high-power applications, such as transport and ship-propulsion drives. In fact, large multiphase machines for ship propulsion have already been prototyped industrially, and are currently undergoing commercial evaluation.

The improved reliability features of multiphase drives, listed at point n°2, enable their use also in faulty conditions, in fact if one phase of a multiphase machine become open circuit, the machine is able to self-start and to run with only a de-rating, which depends on post-fault control strategy and in the number of the phases. In the three-phase case, the loss of one phase determine an important de-rating of the machine while it is running, furthermore the machine is not self-starting and, for this purpose, it requires an external mean. Further details will be given in paragraph 2.5 and 2.6.

Finally, the advantages derived from statement at point n°3 was very important in the 60s, when three-phase inverter-fed ac drives operate with six-step mode. Time-harmonic of voltages and currents introduced by this operation-mode produced low frequency torque ripple, leading to difficulties on speed control and noise production. Since in a n -phase machine torque pulsations are caused by supply time-harmonics of the order $2n \pm 1$, which result in torque ripple harmonic $2n$ times higher than the supply frequency, an increase in

the number of phases seem the best solution to the problem. This aspect of multiphase drives has lost importance since the discover of PWM of VSI, which allows the control of inverter output voltage harmonic content.

Another feature of multiphase machines concerns their efficiency [53], indeed stator windings create a magnetic field in the machine air-gap with a lower space-harmonic content. It results, for two identical machines with the same air-gap field and the same fundamental component of stator current, a reduction of stator Joule losses, hence an increased efficiency. The stator Joule losses saving obtained by increasing the number of phases from three is relatively low. Unlikely, it approaches an asymptote, thus the use of a fifteen-phase machine instead of twelve-phase one produces a stator Joule losses save of only 0.2% [1].

Some of the aforementioned technical characteristics are nowadays still as relevant as they were in the early days, such as that one at point n°1 and at point n°2 of the previous list. Over the years, multiphase drive characteristics have been explored more in details and other beneficial features have been recognized, such as the possibility to enhance the drive torque capability [54], [55] and the opportunity to realize a multiphase multi-motor drive system with single inverter supply [56].

The two latter aspects, together with the fault tolerant feature, appear as natural solutions for some industrial problems, thus they will be described more in details in the following paragraphs.

All the features above presented are suited both for multiphase rotary machine and for multiphase linear ones.

2.5 Multiphase drives for torque capability enhancement

A possible way to use the large number of degrees of freedom of multiphase drives consists in the utilization of the spatial third harmonic component of the flux density in the air gap for increasing the torque production capability. This feature could be particularly interesting in applications where volumetric or weight constraints are important, indeed for a given torque value, the volume and the weigh of the multiphase machine controlled as stated above are smaller than the ones of the three-phase motor.

The relation between time and space-harmonic fields produced by a multiphase winding presented in [53] explains clearly the increasing torque capability feature. Under the hypothesis of stator current with fundamental component of frequency f together with time-harmonic components at integer multiples of f , the excited $2P$ pole n -phase stator winding can be modelled by blocks of current and then resolved into rotating harmonic surface current distributions, thus it results of the form:

$$J_s(\theta, t) = \text{Re} \sum_k \sum_v \sqrt{2} \bar{J}_s^{kv} e^{j(k\omega t - vP\theta)} \quad (2.14)$$

where:

$$\omega = 2\pi f \quad (2.15)$$

In (2.14), k is a positive integer which ranges over all time harmonics produced by the inverter, and θ is the azimuthal co-ordinate. The rms phasor of stator surface current density is represented by \bar{J}_S^{kv} , it has $2\nu P$ poles and rotates at a speed of $k\omega = \nu P$ radians per second with respect to the stator.

The expression for \bar{J}_S^{kv} is:

$$\bar{J}_S^{kv} = \frac{n I_k Z}{\pi D} K_{dv} K_{pv} \quad (2.16)$$

where Z is the number of series-connected conductors per phase, I_k is the k -th time-harmonic component of phase current, and D is the mean air-gap diameter. Pitch and distribution factor for the ν -th harmonic are respectively K_{dv} and K_{pv} .

It is shown in [53] that \bar{J}_S^{kv} is non-zero only for values of ν that are related to k and to the phase number n by the expression:

$$\nu = k - 2ni \quad i = 0, \pm 1, \pm 2, \pm 3, \dots \quad (2.17)$$

Equation (2.17) contains the basic information about the time and space harmonic fields produced by an n -phase excitation. In a five-phase machine ($n = 5$), the fundamental frequency excitation ($k = 1$) produces space-harmonic fields of order $\nu = 1, -9, +11, \dots$ whereas the third time-harmonic ($k = 3$) produces space-harmonic fields of order $\nu = 3, -7, +13, \dots$. It is shown that the fundamental time-harmonic in excitation controls the fundamental space-harmonic in the air-gap of the machine, moreover the third time-harmonic in excitation controls the third space-harmonic.

The independent control of the first and third spatial harmonic component of the magnetic field in the air gap of a machine with concentrated windings (one slot per pole per phase, i.e. $q=1$) can be used to synchronize the third spatial harmonic with the first one in order to obtain an air-gap flux density nearly trapezoidal, leading to back-EMF voltages having non-sinusoidal waveforms, so that the torque per ampere can be increased by 10% [53], [55], [57]. A high performance induction motor drive with high torque density can be obtained using an "Extended Field Oriented Control" [58], [59] or an "Extended Direct Torque Control" [60].

Furthermore, multiphase PM synchronous motors with surface mounted magnets in the rotor have a nearly rectangular air-gap flux density distribution, whereas the armature is realized with fractional slot windings in order to minimize the cogging torque effect. Nevertheless, the use of concentrated winding with a full-pitch is able to maximize the torque per ampere. These motors have the advantages of both BLDC (rectangular-fed brushless dc motors) motors and PMSMs (sinusoidal fed PM synchronous motors). This means that it has the controllability of a PMSM while having the high torque density of a BLDC motor [61].

2.6 Fault tolerant drives

The increased number of phases in multiphase drives offers considerable benefits because of the capability to continue operation when a single or multiple phase loss occurs [62].

Three-phase drive is sensitive to different kinds of faults, both in motor phase and in inverter leg. When one of these faults does occur in one phase, the drive operation has to be stopped for a non-programmed maintenance schedule. The motor in faulty conditions is able to run but it is not still self-starting. The cost of this schedule can be high, thus justifying the development of fault tolerant motor drive systems.

On the contrary, multiphase machines in post-fault condition can continue to be operated with an asymmetrical winding structure and unbalanced excitation, producing a higher fraction of their rated torques with little pulsations when compared to the three-phase machines [63], [64], [65].

Such a feature is very useful in safety critical applications, where the whole system reliability has to be high, even when a fault occurs. Applications which use the “by wire” technology, naval propulsion systems, “more-electric” aircraft and electric and hybrid vehicles are typical examples.

Fault tolerant feature can be easily obtained in multiphase machine designed as n -phase machine composed of b groups or windings of a -phase systems [66], [67], [68]-[69]. The whole motor has $n=ab$ phases, but exists b isolated neutral points and each a -phase system is fed by b a -phase drives. The post-fault strategy for this kind of motor is very simple, the a -phase winding in which the fault has occurred is disconnected, whereas the remaining a -phase windings can continue to operate without any control algorithm modification. The torque and power de-rating coefficient for every a -phase system detached is $(b-1)/b$.

A multiphase machine with single neutral point allows to fully exploit the degrees of freedom of multiphase drives, thus it offers better characteristics in post-fault operations than the multi-neutral point solution [70]. The exclusion of only the faulty phase within the possibility to continue to operate the healthy phases, leaving out problems related to fault isolation, permits to minimize the torque and power de-rating. Indeed, for a given n -phase

motor, the single neutral point solution permits the exclusion of the only faulty phase, whereas in multi-neutral point solution is necessary to take out of service the a -phase system which contains the faulty phase, thus a phases are detached.

The control strategy for post-fault operation in a single neutral point machine has to determine the relations between the currents in the remaining healthy phases in order to pursue a specific aim. The effect of the strategies used, for a given multiphase drive, depends on the load operating point and on the load torque characteristic. Keeping magnitude and phase of the currents in the remaining un-faulted phases at their pre-fault values, it results in a stator joule losses reduction by a factor $(n-1)/n$ and a consequential reduction in developed torque, but the slip increase along with the rotor loss. This easy control strategy, does not exploit the whole number of degrees of freedom of the multiphase drive.

An alternative solution can allow an increase in the magnitude of the current in each un-faulted phase. Hence, the whole stator joule loss remains at its pre-fault value and low torque pulsations result. This solution gives both a smaller drop in speed and a smaller rotor joule losses than the previous strategy.

A third strategy could pursue the aim to maintain the torque and the power at their pre-fault value. An increase of the magnitude of the current in each un-faulted phase, higher than the previous strategy, is necessary; consequently it determines also an increase in stator joule losses. Thus this solution is not suited for operations sustained for a long period of time, since overheating problems reveal.

The practical implementation of any of these strategies might prove other problems, such as to the rating of the power electronic switches and the limitation imposed by the DC link voltage.

2.7 Multi-Motor drives

Another possibility offered by multiphase drives is related to the so-called multi-motor drives. A well-defined number of multiphase machines, having series connected stator windings with an opportune permutation of the phases, as shown in Figure 1, can be independently controlled with a single multiphase inverter [71]-[72].

A vector control algorithm can be applied to each machine separately to generate the inverter leg control signals, and to supply the stator windings of the multi-machine system from a single current controlled by a voltage source inverter (VSI). Inverter current control is performed in the stationary reference frame, using inverter phase currents. The number of multiphase motors connected in series, or rather the number of driving axles, depends on the number of the phases of the multiphase inverter. The maximum number of motor connectable in series, for a system with n -phases, is $M = (n - 2) / 2$, in case of n is a even number, while it is $M = (n - 1) / 2$ if n is an odd number.

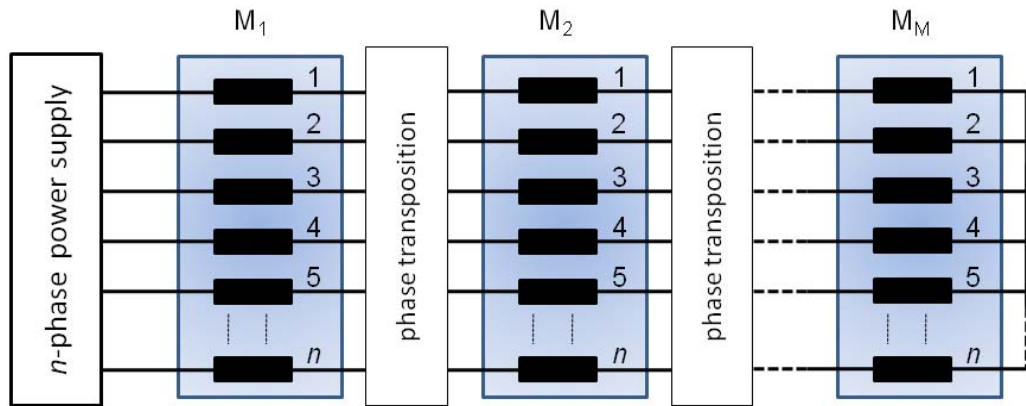


Figure 1-Conceptual winding connections of $(n - 1) / 2$ machines in multi-motor drives supplied by a n -phase inverter.

The necessity to control several electrical machines with a coordinated motion is an usual requirement in automatic industrial applications. Some examples are the X-Y placer, high-speed packaging machine, pick-and-place machine used for electronic boards and silicon mono-crystal production equipments.

The traditional solutions use three-phase drives, or rather one three-phase motor fed by one inverter for each driven axle shown in Figure 2. The control architecture of such a system can be centralized or decentralized. In the first case the control of each motor is elaborated by a central control unit or by one control unit belonging to a more complex hierarchical control system, and each inverter behaves in many cases as a power amplifier of the control signals elaborated by the centralized control. In the second case the control of

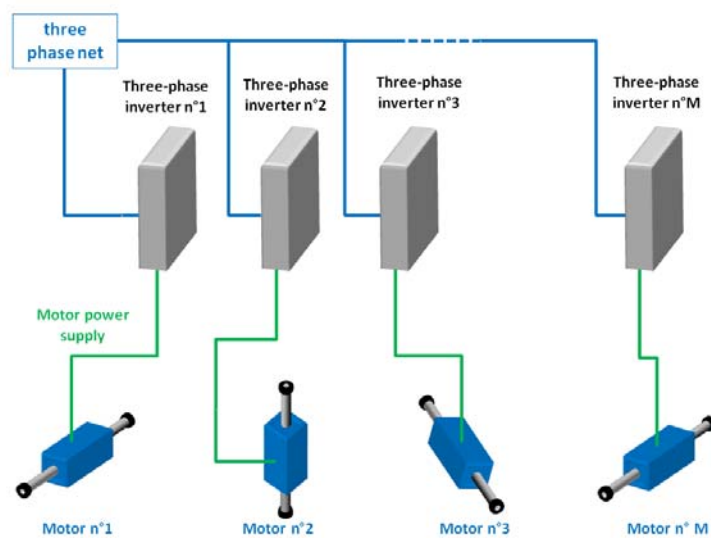


Figure 2-Multi-motors configuration with three-phase drives.

each motor is directly implemented on its own inverter, and the motion synchronization among the whole driving axles is managed by one “master” drive through an electronic cam.

Taking into account the power connection point of view, each inverter can be fed by the three-phase grid or can be connected to a DC link as shown schematically in Figure 3, enabling a complete energy recovery system.

Multiphase multi-motors drives provide different solutions rather than the three-phase one, both for power feature and for control structure. The former results in a hardware saving, indeed taking as example a two-motor drives, it results that the minimum inverter leg number required for multiphase solution is five, whereas the classical three-phase solutions uses six inverter legs. The hardware saving concerns, besides discrete components of the inverter leg, all the auxiliary circuit and components used to control the components of the leg, such as drivers, protection circuits, electronic power supplies etc. The saving exists for a phase number greater than five, and in general, higher is the number of phases, greater is the number of saved legs is.

Another excellent feature of the multiphase multi-motor drives consists in a control components saving, in fact the implementation of the vector control algorithm for all the motors connected in series can be managed within a single DSP. The control of each motor can be executed in parallel to give the proper control references that, after appropriate summation, results in the phase current control references. If the three-phase solution is considered, one DSP will be used for each drive because each inverter is controlled with a DSP.

The only drawback of multiphase multi-motor drives is an increase of the whole stator winding losses due to the flow of the phase currents through the stator windings of all series connected motors. Considering the situation where only one motor is running, it results in

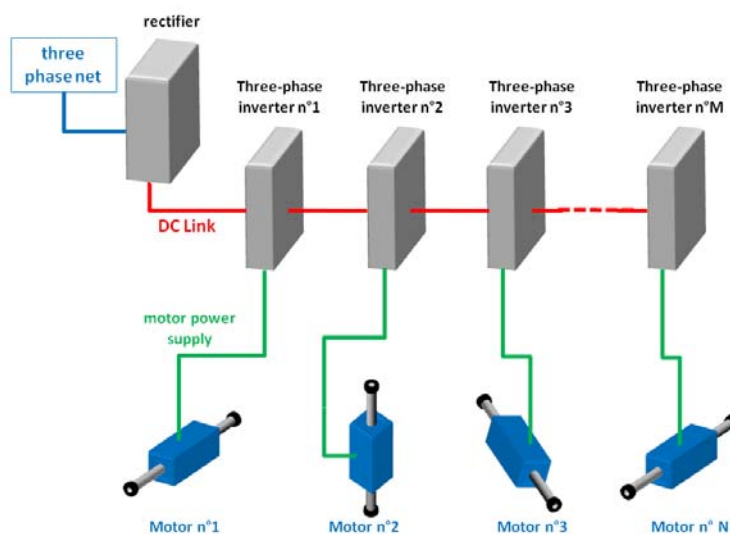


Figure 3-Multi-motors configuration with three-phase drives connected with common DC bus.

stator Joule losses in the motor itself and in the other motors connected in the multi-motor drive. The efficiency of the multi-motor drive decreases when compared to the equivalent three-phase case, but the advantages above discussed seem to overcome the efficiency drawback.

A. Multi-Motor drive concept

Vector control of multiphase machine requires at minimum only two current, i.e. only one space vector current, if only the fundamental field is utilized, as shown by equation (2.12). The additional degrees of freedom offered by multiphase drives can be utilized to control independently other machines within a multiphase multi-motor drive system. There are not any constraints concerning with the motor typologies connectable in series, then the multi-motor drive can be composed of induction and/or permanent magnet synchronous and/or synchronous reluctance motors.

If a machine is designed to produce sinusoidal-field distribution [51], then standard modelling assumption applies and only the first harmonic of inductance terms exists in the phase-variable model. The applications of Clarke's transformation, given in the expression (2.18) for an odd phase number, to the phase voltage equations produces a set of n equations in the stationary frame reference. The first pair of equations is identical to the corresponding one for a three-phase machine, and they are the two components of the first space vector. The last row in (2.18), or the last two rows for even phase numbers, represents the zero-sequence equation. The other couple of rows in expression (2.18), which are $(n-3)/2$ for odd phase number and $(n-4)/2$ for even phase number, correspond to the h -th space vectors, where the space vector index h has the same meaning expressed in (2.3).

As discussed above, the first space vector of the current is the only one able to produce torque/force in the motor. The other current space vectors do not affect the torque/force and their values are influenced by their relative voltage space vectors and the stator winding leakage impedances. These current space vectors represent degrees of freedom that can be used to control other machines connected in series with the first machine. If the control of the machines has to be decoupled one from the other, torque/force producing current space vector of one machine must not produce torque/force in all the other machines in the group. This can be achieved with a proper series connection of the motors, able to transform each current space vector into the first current space vector for its relative motor of the group. In other words, the stator winding connections of multiphase machines must be such that what one machine sees as the first current space vector, the other machines see as h -th current space vector, and vice versa.

In order to do so, it is necessary to connect stator windings of all the multiphase machines in series with an appropriate phase transposition, and finally close all phases of the last motor in star connection, as shown in Figure 1. The necessary phase transposition is taken directly from the Clarke's transformation matrix (2.18), reading it per columns in order

to understand the spatial angle among the rows, which represents the phase step. Thus, phases '1' of all the machines will be connected in series without transposition, indeed the phase step among the rows in column 1 is zero. Phase '2' of the first machine, viz. column 2, has a phase step equal to α ; this means that it will be connected to phase '3' of the second machine, which will be further connected to phase '4' of the third machine and so on. In the same way, phase '3' of the first machine is connected to the phase '5' of the second machine, which further gets connected to phase '7' of the third machine, and so on, because of the phase step is 2. This explanation provides all the information to construct the connection table or connectivity matrix proposed in [56], [75], and reported here in Table I in the general case of a n-phase system. The first column in

Table I shows the machine number connected in series, the first row shows the phase number.

Then it becomes possible to completely independently control the machines while supplying the drive system from a single current-controlled voltage source inverter.

After the description of the main characteristics of multiphase drives, it is worth noting that the multiple space vectors assume different meaning case by case. As an example, in five-phase machines with concentrated windings, the first space vector of the stator currents is responsible of the first spatial harmonic component of the magnetic field in the air gap, whereas the third space vector is related to the third harmonic component [57], [58], [74]. On the other hand, in multiphase multi-motor drives, the first space vector of the output currents is responsible for the first spatial harmonic component of the first machine, whereas the third space vector generates the first spatial harmonic component of the second machine [71].

$$C = \sqrt{\frac{2}{n}} \begin{bmatrix} 1 & \cos(\alpha) & \cos(2\alpha) & \cos(3\alpha) & \dots & \cos(2\alpha) & \cos(\alpha) \\ 0 & \sin(\alpha) & \sin(2\alpha) & \sin(3\alpha) & \dots & -\sin(2\alpha) & -\sin(\alpha) \\ 1 & \cos(2\alpha) & \cos(4\alpha) & \cos(6\alpha) & \dots & \cos(4\alpha) & \cos(2\alpha) \\ 0 & \sin(2\alpha) & \sin(4\alpha) & \sin(6\alpha) & \dots & -\sin(4\alpha) & -\sin(2\alpha) \\ 1 & \cos(3\alpha) & \cos(6\alpha) & \cos(9\alpha) & \dots & \cos(6\alpha) & \cos(3\alpha) \\ 0 & \sin(3\alpha) & \sin(6\alpha) & \sin(9\alpha) & \dots & -\sin(6\alpha) & -\sin(3\alpha) \\ \dots & \dots & \dots & \dots & \dots & \dots & \dots \\ 1 & \cos\left(\frac{\dots}{2}\alpha\right) & \cos\left(\frac{\dots}{2}2\alpha\right) & \cos\left(\frac{\dots}{2}3\alpha\right) & \dots & \cos\left(\frac{\dots}{2}2\alpha\right) & \cos\left(\frac{\dots}{2}\alpha\right) \\ 0 & \sin\left(\frac{\dots}{2}\alpha\right) & \sin\left(\frac{\dots}{2}2\alpha\right) & \sin\left(\frac{\dots}{2}3\alpha\right) & \dots & -\sin\left(\frac{\dots}{2}2\alpha\right) & -\sin\left(\frac{\dots}{2}\alpha\right) \\ \frac{1}{\sqrt{2}} & \frac{1}{\sqrt{2}} & \frac{1}{\sqrt{2}} & \frac{1}{\sqrt{2}} & \dots & \frac{1}{\sqrt{2}} & \frac{1}{\sqrt{2}} \end{bmatrix}$$

(2.18)

Table I-Connectivity Matrix for general n -phase case.

| | A | B | C | D | E | F | G | H | I | L | M |
|-----------|----------|----------|----------|----------|----------|----------|----------|----------|----------|----------|----------|
| M1 | a | b | c | d | e | f | g | h | i | l | ... |
| M2 | a | b+1 | c+2 | d+3 | e+4 | f+5 | g+6 | h+7 | i+8 | l+9 | ... |
| M3 | a | b+2 | c+4 | d+6 | e+8 | f+10 | g+12 | h+14 | i+16 | l+18 | ... |
| M4 | a | b+3 | c+6 | d+9 | e+12 | f+15 | g+18 | h+21 | i+24 | l+27 | ... |
| ... | ... | ... | ... | ... | ... | ... | ... | ... | ... | ... | ... |

B. Machine connectivity

The phase number n influences the number of connectable machines and their individual phase numbers. This issue is well described in [75], where the multi-motor drive is divided in three categories detailed as follows.

- 1) The number of phases n is a prime number, then the number of machines connected in series with phase transposition is:

$$M = \frac{(n-1)}{2} \quad (2.19)$$

It corresponds to the number of independent space vectors obtained with transformation (2.3). Every machine of the group has a number of phases equal to n . Example of multiphase systems that belong to this category are $n=3, 5, 7, 11, 13, 17, 19$, etc.

- 2) The number of phases does not belong to the previous category, but it can be calculated as:

$$n = l^m \quad (m = 2, 3, 4, \dots) \quad (2.20)$$

The number of machines in series is still calculated with (2.19), but not all M machines have n phases. For example, with a nine-phase system, the multi-motor drive is composed of $M=4$ machines: one of them is a three-phase machine, whereas

the remaining three machines have nine phases. The connection diagram for this case is shown in Figure 4. For the general case of $m > 1$, the machines of the series have a number of phases which belong to the following succession (2.21):

$$n, \frac{n}{l}, \frac{n}{l^2}, \dots, \frac{n}{l^{m-1}} \tag{2.21}$$

Multiphase systems belonging to this category have a number of phases $n = 9, 25, 27, 49, 81$, etc.

- 3) The number of phases does not belong to the category listed at point n°1 and n°2. However, n is divisible by two or more prime numbers, denoted as n_1, n_2, n_3 , etc. Then $n = n_1 \cdot n_2 \cdot n_3 \dots n_j$. Thus, the maximum number of machines connectable in series is calculated by (2.22):

$$M < \frac{(n-1)}{2} \tag{2.22}$$

Ordering rules require that all the n -phase machines are at first connected in series to the source, with phase transposition. Then all the other machines follow, ordered with a decreasing phase number. Thus, if the sequence of the largest prime number which divides n is n_1, n_2, n_3, \dots , then the sequence of the motors connected in series is ordered as the prime number sequence. The observation of this rule permits the series connection of the whole group of motors, otherwise it should be impossible to

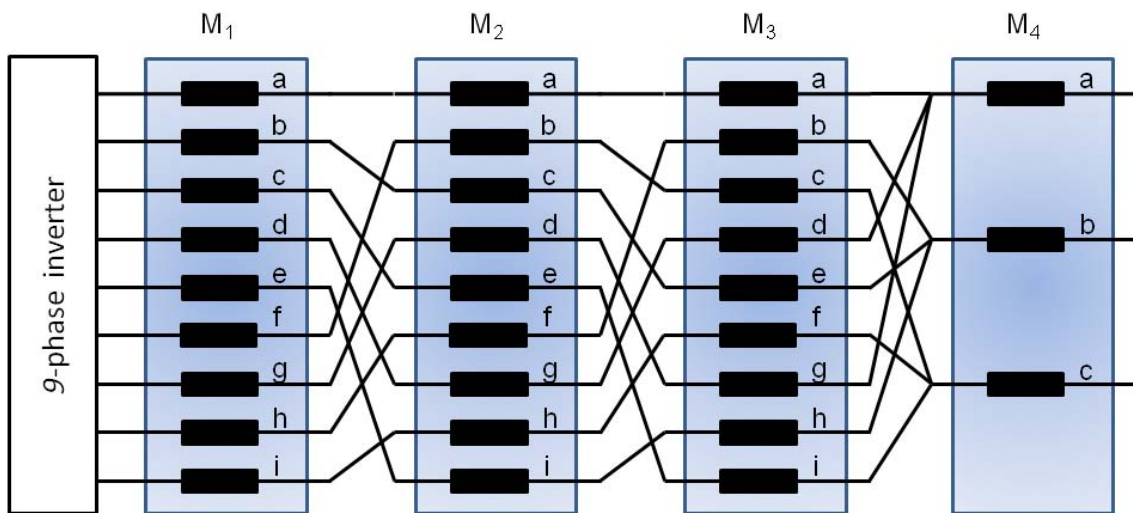


Figure 4-Connection diagram with phase transposition for the nine-phase case.

connect a motor with higher number of phases after a lower phase number machine. Thus the latest n -phase machine has to be connected with the first n_1 -phase machine, the latest n_1 -phase machine has to be connected with the first n_2 -phase machine, and so on. The connection of machines with different prime numbers, such as n_1 and n_2 , seems to be impossible, since the ratio n_1/n_2 is not a integer number. An attempt to connect these kind of machines leads to the short-circuiting of some terminals. The group of machines will be composed of motors with different phase number, in general the machine phases are equal to n and one of the prime number n_1, n_2, n_3 , etc.

That is, the number of phases of machines are n, n_1 or n, n_2 or n, n_3 or n, \dots or n, n_j .

This class of odd phase numbers encloses the situation where, besides the same prime number, there is at least one other prime number in the sequence, such as $n = n_1 \cdot n_2 \cdot n_3 \cdots n_j \cdot l^m$. The phase numbers belonging to this category are $n = 15, 21, 33, 35, 39, 45, 51, 55, 57, 63, 65, 69, 75, 77$, etc.

Categories at point n°2 and n° 3 of the list can be considered a sub-categories of a more general case, where n is not a prime number. The common feature among these two categories is that the series connection is composed with motors with two or more phase numbers.

C. Control

The torque/force produced by a n -phase PM synchronous machine is directly controllable through the current space vectors, as shown in (2.11). A machine designed for multi-motor drive has to produce sinusoidal-field distribution in the air-gap in order to make the machine controllable through the only first current space vector, whereas the other current space vectors must not influence torque/force, viz. the motion control. Current control VSI is thus required to supply the multi-motor system with decoupled control of each motor. Any of the available vector control algorithm is applied in conjunction with each machine in order to generate individual machine phase current references, which are further summed in an appropriate way to obtain the inverter phase current references. Vector control of multi-motor drives can be achieved by using either current control in the stationary reference frame or in the rotating reference frame [73]. The latter shows in [76]-[77] an increased parameter sensitivity. This happens since the decoupling voltages become functions of parameters of both machines, due to the need for compensating voltage drops in one machine caused by the flow of the torque/force producing currents of the other machine through out its windings. Thus, control in the stationary reference frame is better suited series-connected multiphase multi-motor drive systems.

2.8 Conclusion

Multiphase drives have large number of degrees of freedom if compared to the classic three-phase system. Though the multiphase drive concept is not new, it has attracted the attention of the research community since the 90s. Thus, new features have been developed, such as the drive power capability enhancement, fault-tolerant characteristics and, last but not least, the multi-motor drive configuration. The latter represents an interesting and promising solution for automatic machine where coordinated motion control among several motors is required. Then it will be investigated in the following chapters.

CHAPTER 3

PM Tubular Motor modelling and optimized design algorithm

3.1 Introduction

An optimal design of PM tubular linear actuators permits to fully exploit the limits of soft and hard magnetic material, resulting in high performance motors. This objective can be reached paying attention not only to the electromagnetic issues, but also to the thermal and mechanical constraints.

An integrated electromagnetic, thermal and mechanical design is developed in order to maximize the thrust force or the dynamic performance of a series of PM tubular linear actuators. Furthermore, the dynamic behaviour of the motor is very important due to the inherent reciprocating motion of the mover, thus an optimized number of wires per slot is determined through numerical simulations which take into account also the inverter constraints.

3.2 Review of design optimization methodologies

A variety of techniques has been employed to facilitate the design optimization, prediction of magnetic field distributions through analytical field computation was carried out in [78], [79], [4], whereas the most common approach employs a lumped equivalent circuit [80], [81], [82], [83], finally Finite Element Method (FEM) represents another analysis tool. The first one gives good calculation results of field distribution and thrust force, considering also cogging force effect, but it does not allow to manage the relationship between critical design parameters and machine performance, as happens with the second methodology. Finally, FEM analysis provide an accurate mean to determine the field distribution, that takes into account the saturation, but it remain time consuming.

It does not exist a better solution, because each technique have merits and demerits, depending also on the motor design constraints and in the motor topology.

3.3 Electromagnetic model

The structure of the PM tubular actuator is shown in Figure 1. The slider is constituted by a tube containing axially magnetized Nd-Fe-B magnets alternated with ferromagnetic disks. The stator is composed of a magnetic yoke, and several inner disks. The stator windings, placed between the disks, have the form of cylindrical coils.

A. Preliminary considerations

In order to define an optimized algorithm, the main technical issues of tubular linear actuators have to be considered.

Magnetic circuit lamination cannot be adopted because of the 3D flux paths, but the use of Soft Magnetic Composites (SMCs) can solve the problem to mould the yoke, the stator inner rings and the slider poles. Although SMCs have lower strength, higher losses at low frequencies and lower maximum permeability than laminations, insulated iron powders present isotropic magnetic properties combined with the possibility to mould complex 3D magnetic circuits.

A preliminary machine design can be carried out on the basis of a simplified one-dimensional field analysis in order to determine the main actuator dimensions, once some key-parameters are prefixed. This allows, for given volume specifications, the determination of the main actuator dimensions and performance, considering thermal and mechanical issues.

B. Thrust force contributions

In the actuator topology shown in Figure 1, the constant component of the thrust force is produced by the permanent magnet and winding current interaction. There is also an additional constant component of force, the reluctance force, due to the varying reluctance of the magnetic circuit. In this type of actuators, there are four sources of the force ripple:

- 1) the cogging effect, i.e. the tendency of permanent magnets to align with the stator teeth at positions where the reluctance of the magnetic circuit is minimized,
- 2) the end-effects, due to the open magnetic circuit nature,
- 3) the presence of harmonics in the air-gap flux density distribution of the permanent magnets,
- 4) the presence of high order harmonics in the reluctance of the magnetic circuits.

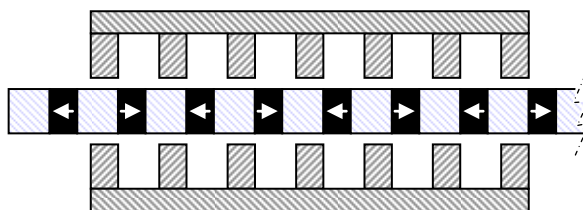


Figure 1-Basic scheme of a tubular permanent magnet motor with axial magnets.

The first contribution produces the cogging force, the second contribution the so-called end-effect force, and the third contribution is responsible of the field harmonic electromagnetic force. The causes of force pulsations coming from the PWM supply are not considered in this paper.

Unfortunately, the traditional methods used in rotary PM brushless machines to reduce the cogging torque, i.e. use of skewed or asymmetrical distributions of the permanent magnets [34], are not easily applicable in tubular machines. As a consequence, in these types of machines, the cogging force can be reduced acting only on the geometries of stator slots, magnets and slider poles.

The end-effect force, instead, can be compensated adding ferromagnetic disks in one or in both extremity of the stator assembly: this aspect will be discussed paragraphs 3.6, section D.

C. Fundamental hypothesis

Some hypothesis has used to simplify the definition of the model equation for the considered actuator topology. In particular, it has been assumed:

- one-dimensional field analysis;
- infinite iron permeability;
- cylindrical symmetry;
- negligible end effects;
- negligible iron saturation.

Despite some of the afore-listed assumptions seem to be very restrictive, they results from approximations suitable for the kind of motor analyzed. The statement in the first point simplifying the problem modelling, whereas the simplification stated in the second point consider that PM tubular machines have low natural permeance due to presence of magnets, thus the iron reluctance is less important and can be neglected. The cylindrical symmetry listed in the third point is a inherent properties of the motor. The end-effect can be neglected as stated in the fourth point if proper strategies are used. Finally, iron saturation does not occur when the machine is designed such that the magnetic load is in the linear part of the first-magnetization curve of iron.

D. Design of the magnets

The main geometric parameters used to define the electromagnetic model of the motor are depicted in Figure 2.

The magnetization curve of the Nd-Fe-B magnet can be expressed by the following relationship

$$B_m = \mu_r H_m + B_r \tag{3.1}$$

where B_m is the magnet flux density in axial direction, H_m the magnetizing force, B_r the magnet remanence and μ_r the magnet permeability.

The magnet diameter can be related to the pole pitch by equating the slider core flux to the air-gap flux as follows

$$2(B_m \frac{\pi}{4} (d_{si}^2 - d_{sib}^2)) = B_g \pi d_g t_p \tag{3.2}$$

where t_p is the pole pitch, B_g is the air-gap flux density calculated in the mean diameter d_g , the latter defined as

$$d_g = d_{si} + 2h_t + g \tag{3.3}$$

The magnet width can be expressed in terms of the air-gap flux density and magnet magnetizing force as follows:

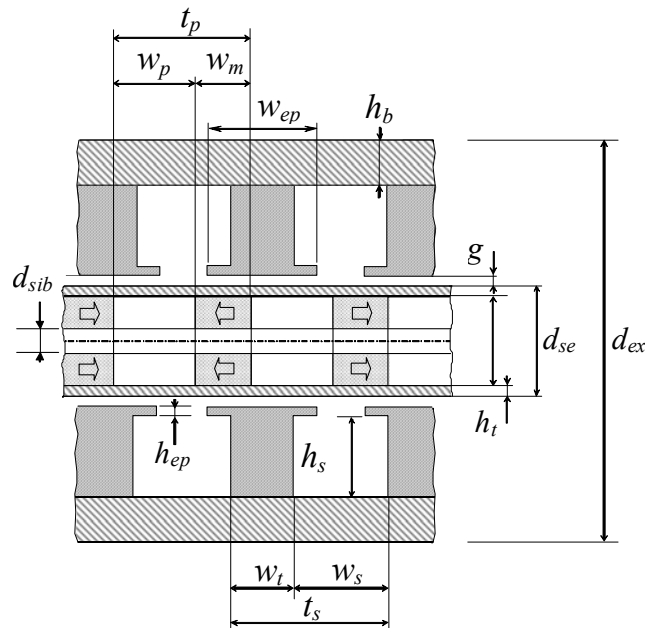


Figure 2-Drawing of the tubular actuator showing the geometrical parameters.

$$w_m = -\frac{2}{H_m} \frac{B_g}{\mu_0} \delta_0 K_C \quad (3.4)$$

where δ_0 is the magnetic air-gap given by

$$\delta_0 = h_t + g \quad (3.5)$$

and K_C is the Carter's coefficient that takes the stator and slider slot effect into account. It can be expressed by

$$K_C = \frac{t_s}{t_s - \frac{(t_s - w_{ep})/\delta_0}{5 + ((t_s - w_{ep})/\delta_0)} \delta_0} \frac{t_p}{t_p - \frac{(w_M/\delta_0)^2 \delta_0}{5 + (w_M/\delta_0)}}. \quad (3.6)$$

E. Slider and stator design

The slider core flux density B_p can be related to the magnet flux density by

$$B_p \pi d_{si} w_p = 2 (B_m \frac{\pi}{4} (d_{si}^2 - d_{sib}^2)). \quad (3.7)$$

The tooth flux is equal to the pole flux divided by the number of teeth in a pole pitch, and can be expressed as

$$\varphi_t = B_g \pi d_g t_p / N_{sp} \quad (3.8)$$

where

$$N_{sp} = N_s / N_p. \quad (3.9)$$

The radial cross-sectional area of a polar shoe facing the air-gap and that of the tooth can be calculated respectively by

$$A_{ep} = \pi (d_g + g) w_{ep} \quad (3.10)$$

and

$$A_t = \pi (d_g + g + 2h_{ep}) w_t \cdot \quad (3.11)$$

The tooth flux density is

$$B_t = \frac{\varphi_t}{A_t} = \frac{B_g d_g t_p}{w_t (d_g + g + 2h_{ep}) N_{sp}} \quad (3.12)$$

whereas the stator pole shoe flux density results

$$B_{ep} = \frac{\varphi_t}{A_{ep}} = \frac{B_g d_g t_p}{w_{ep} (d_g + g) N_{sp}} \cdot \quad (3.13)$$

The slot width can be calculated as follows:

$$w_s = w_{act} / N_s - w_t \quad (3.14)$$

where w_{act} is the total actuator length.

Taking into account the pole flux to back iron flux ratio, assuming the tooth flux density equal to the slider core flux density, the cross-sectional area of the back iron is given by

$$A_b = A_t N_{sp} / 2 \quad (3.15)$$

and the back iron height becomes as follows:

$$h_b = \frac{A_b}{\pi (d_{se} + 2g + 2h_s + h_b)} \cdot \quad (3.16)$$

Finally, the slot height can be expressed by

$$h_s = \frac{1}{2} (d_{ex} - d_{se} - 2g - 2h_b) \quad (3.17)$$

F. Thrust force calculation

The thrust force can be calculated as follows:

$$F = \frac{I}{v_s} \sum_{k=1}^3 \frac{d\varphi_k}{dt} i_k \quad (3.18)$$

where φ_k is the magnet flux linked with the k -th phase, i_k is the corresponding line current and v_s the slider speed.

Assuming sinusoidal winding currents, a thrust force is constant when also the induced EMFs are sinusoidal. Applying Steinmetz's transformation to (3.18) leads to the following expression of the thrust force:

$$F = \frac{I}{v_s} \sum_{k=1}^3 j\omega \bar{\Phi}_k \cdot \bar{I}_k \quad (3.19)$$

The slider speed in (3.20) is related to the angular frequency of the supply voltage as follows:

$$v_s = \omega \frac{t_p}{\pi}. \quad (3.20)$$

The maximum value of the coil flux linkage can be calculated as

$$\Phi_c = \frac{B_g \pi d_g t_p}{2 N_{sp}} \quad (3.21)$$

and the maximum value of the phase flux linkage is

$$\Phi_M = N_g n Q K_d \Phi_c \quad (3.22)$$

where N_g is the number of series-connected groups of coils, Q is the number of coils per group, n is the number of wires per coil, and K_d is the winding factor.

The current density can be expressed in term of Joule losses and geometric parameters by

$$J = \sqrt{\frac{P_{cu}}{\rho N_s \pi (d_{si} + 2\delta + h_s) w_s h_s K_s}} \quad (3.23)$$

where P_{cu} is the winding losses, K_s is the slot fill factor and ρ is the copper resistivity. It is worth noting that the value of P_{cu} in (3.23) should be chosen taking into account the cooling capability of the tubular actuator.

The peak value of the total slot current value is

$$I_c = \sqrt{2} w_s h_s K_s J. \quad (3.24)$$

Finally, assuming that the machine operates in field oriented control conditions, the electromagnetic thrust force can be expressed as

$$F = \frac{3}{2} \frac{\pi}{t_p} \Phi_M \frac{I_c}{n} \quad (3.25)$$

3.4 Thermal model

The thermal analysis allows to verify the compatibility between the temperatures inside the actuator and the selected insulation class. The thermal analysis can be performed by means of lumped equivalent thermal circuit or FEM analysis of the temperature distributions.

The first method is particularly suitable in the preliminary design to determine the average temperature of different inner parts of the actuator, but the precision of the results is influenced by the accuracy of the lumped circuit schematization.

For simplicity, the temperature of the frame, moulded in aluminium or cast iron, can be considered uniform because of the high value of thermal conductivity coefficient. Considering the actuator fixed on an adiabatic surface, with the simplified frame shape depicted in Figure 3, and with the slider in horizontal position, the frame-to-environment temperature rise \mathcal{G}_{f-e} can be calculated by means of the following equation:

$$Q_{tot} = \frac{\mathcal{G}_{f-e}}{R_{conv}} + Q_{rad} \quad (3.26)$$

where Q_{tot} is the total power losses, R_{conv} the thermal frame-to-environment resistance due to natural convection, and Q_{rad} the radiated thermal power. R_{conv} can be expressed as follows:

$$R_{conv} = \frac{1}{\alpha_{vc} S_V + \alpha_{hc} S_H} \quad (3.27)$$

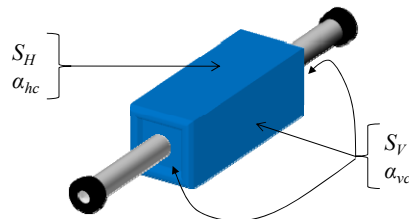


Figure 3-Simplified frame shape used for thermal modelling.

where S_V and S_H are the values of the vertical and horizontal frame surfaces, whereas α_{vc} and α_{hc} are the natural convection coefficients for vertical and horizontal surfaces. The values of α_{vc} and α_{hc} can be calculated as follows:

$$\alpha_{vc} = 5.6 \sqrt[4]{\frac{\mathcal{G}_{f-e}}{h T_{env}}} \quad (3.28)$$

$$\alpha_{hc} = 0.5 \alpha_{vc} \quad (3.29)$$

where h is the frame height and T_{env} the ambient absolute temperature.

Finally, the radiated power can be calculated as follows:

$$Q_{rad} = \sigma_{rad} S_{rad} \left[(T_{env} + \mathcal{G}_{f-e})^4 - (T_{env})^4 \right] \quad (3.30)$$

where σ_{rad} is the frame radiation coefficient and S_{rad} is the radiation surface value, calculated as the sum of S_V and S_H .

Under the assumption of winding losses uniformly distributed in the coils, the average value of the winding-to-frame temperature rise can be expressed as

$$\mathcal{G}_{w-f} = \frac{P_{cu}}{N_s S} \left(\frac{s}{\lambda'} + \frac{2}{3} \frac{w_s - 2s}{4\lambda} \right) \quad (3.31)$$

where s is the thickness of the slot insulation, S is the lateral surface of the winding, λ is the thermal conductivity of the slot insulation, and λ' is the equivalent thermal conductivity of the winding, depending on the enamelling, the impregnation and the fill factor of the slot. The main slot parameters are highlighted in Figure 4, where a axial sight of the motor is shown (a) and a 3-D view of one winding is depicted (b).

Finally, the winding-to-environment temperature rise is

$$\mathcal{G}_{w-e} = \mathcal{G}_{w-f} + \mathcal{G}_{f-e} \quad (3.32)$$

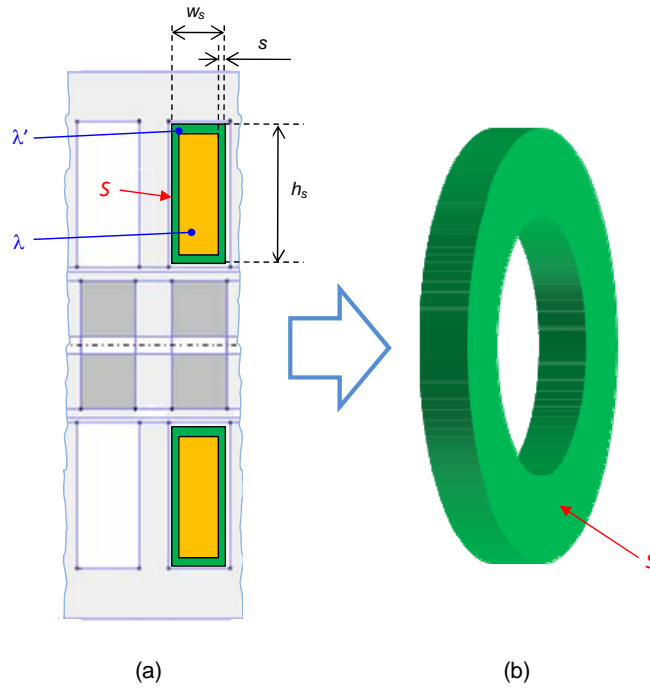


Figure 4-Drawing of the tubular actuator showing the geometrical parameters of one highlighted coil (a), and 3D sight of the coil (b).

3.5 Mechanical model of the slider

The slider of tubular PM motors usually presents a slight eccentricity with respect to the symmetry axis of the stator, due to the assembling misalignment and clearance of the bearings [84]-[85]. As a consequence, the resultant radial force acting on the slider, due to the magnets, is not zero and the static equilibrium configuration of the slider axis tends to bend. The calculation of the maximum displacement of the slider axis is extremely important in order to verify that there is no interference between slider and stator. In addition, the reaction forces on the bearings have to be determined, because they increase the friction reducing the life of the actuator.

The analysis of the static equilibrium configuration of the actuator is reported under the assumption of elastic materials and small displacements.

A. Static equilibrium analysis

To analyze the static equilibrium of the slider, it is convenient to use the scheme of a simply-supported beam loaded with a distributed force q , shown in Figure 5. As known, the static equilibrium equation of the deflected beam is as follows:

$$-EI \frac{d^4 v(z)}{dz^4} + q(z) = 0 \tag{3.33}$$

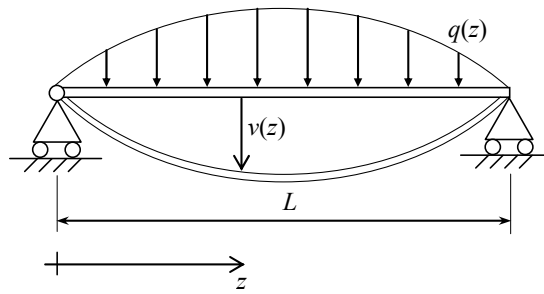


Figure 5-Scheme of the simply-supported beam for the study of the slider static equilibrium configuration .

The bending moment $M(z)$ is related to the displacement v as follows:

$$M(z) = -EI \frac{d^2v(z)}{dz^2} \quad (3.34)$$

Equations (3.33) and (3.34) can be solved imposing the boundary conditions that $v(z)$ and $M(z)$ vanish for $z=0$ and $z=L$ once the distributed load q is known.

In order to determine q , reference is made to Figure 6, showing a transverse section of the tubular actuator, where the slider is located in an eccentric position with respect to the stator symmetry axis. Under the assumption of small displacements, the magnetic gap can be expressed as follows:

$$\delta = \delta_0 + y \cos \theta. \quad (3.35)$$

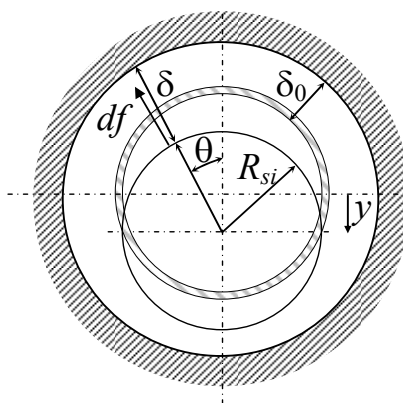


Figure 6-Transverse section of the tubular motor showing the eccentricity of the slider.

The elementary force acting on the elementary surface dS of the slider is:

$$df(\theta) = \frac{B(\theta)^2}{2\mu_0} dS. \quad (3.36)$$

The distributed force q , resultant of all elementary contribution, is directed downwards and is given by

$$q = -\int_0^{2\pi} d_{si} \frac{B(\theta)^2}{4\mu_0} \cos(\theta) d\theta. \quad (3.37)$$

To explicit the expression (3.37), the function $B(\theta)$ has to be determined. Considering the motor section depicted in Figure 7 and calculating the MMF drop along the dashed line it follows:

$$B(\theta) = \frac{1}{2} \mu_0 \frac{W_M H_M}{\delta(\theta)}. \quad (3.38)$$

Substituting (3.35) in (3.38), the resulting equation can be expressed in Mc Lauren's series, as follows:

$$B(\theta) = B_0 \left(1 - \frac{y}{\delta_0} \cos \theta + \dots \right) \quad (3.39)$$

where $B_0(z)$ is the value of the flux density in the original configuration. Substituting (3.39) in (3.37) leads to the following expression of $q(z)$:

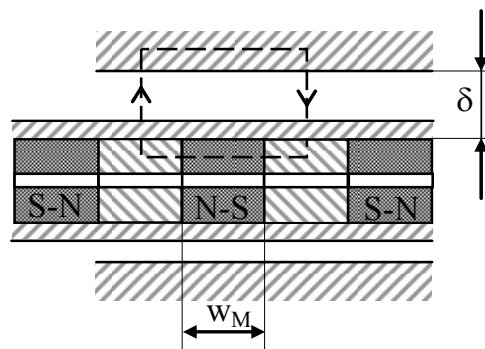


Figure 7-Longitudinal motor section.

$$q = \frac{\pi R_{si} B_0^2}{2 \mu_0 \delta_0} y. \quad (3.40)$$

In order to take the non-uniformity of the magnetic field in the actuator into account, it can be demonstrated that in (3.40) B_0 can be approximated by B_{RMS} . In addition, the displacement y can be expressed as the sum of two terms, namely the eccentricity v_0 and the displacement v due to bending. In this way, the distributed load q becomes:

$$q = \frac{\pi R_{si} B_{RMS}^2}{2 \mu_0 \delta_0} (v + v_0). \quad (3.41)$$

Substituting (3.41) in (3.33) and solving the differential equation it is possible to obtain the analytical expression of $v(z)$. Adding the maximum value of $v(z)$ to the initial eccentricity v_0 leads to the maximum displacement y_{max} of the slider axis.

B. Maximum slider displacement

Assuming that v_0 is the eccentricity of the slider axis with respect to the symmetry axis of the stator, the maximum displacement of the slider can be expressed as

$$y_{max} = \alpha v_0 \quad (3.42)$$

where α is a coefficient greater than 1 defined as

$$\alpha = \frac{1}{2} \left[\left(\cosh \frac{KL}{2} \right)^{-1} + \left(\cos \frac{KL}{2} \right)^{-1} \right]. \quad (3.43)$$

In (3.43) L is the distance between the bearings and K is defined as follows

$$K = \sqrt[4]{\frac{\pi R_{si} B_{RMS}^2}{2 \mu_0 \delta_0 E I}} \quad (3.44)$$

where B_{RMS} is the RMS value in a pole-pitch of the spatial distribution of the flux density, E is the Young's modulus and I is the moment of inertia of the slider tube with respect to the bending axis.

The behaviour of α is shown in Figure 8 as a function of the product KL . According to (3.42), the maximum displacement is proportional to the slider eccentricity. Therefore attention has to be paid to the choice of bearings type and the assembling accuracy.

Finally, it is worth noting that if KL is a multiple of π , then (3.42) has an infinite value, i.e. a static equilibrium configuration is not possible. The case $KL=1$ gives the critical distance between the bearings, that is

$$L_{cr} = \frac{\pi}{K} = \sqrt[4]{\frac{\mu_0 \delta_0 \pi^3 E I}{R_{si} B_{RMS}^2}} \quad (3.45)$$

Obviously, the stator length should be far enough from the critical length L_{cr} in order to avoid interference between stator and slider.

C. Reaction forces on the bearings

The resultant force R due to the radial magnetic forces can be calculated by means of the following equations:

$$R = \beta \frac{\pi d_{se} B_{rms}^2}{\mu_0 \delta_0} v_0 L \quad (3.46)$$

where β is a constant greater than 1, depicted in Figure 9, whose expression is as follows:

$$\beta = \frac{1}{KL} \left(\tanh \frac{KL}{2} + \tan \frac{KL}{2} \right) \quad (3.47)$$

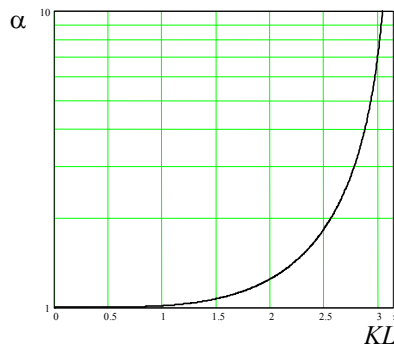


Figure 8-Behavior of the parameter α .

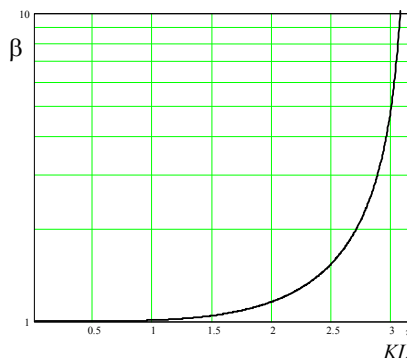


Figure 9-Behavior of the parameter α .

The reaction forces on the bearings are equal to $R/2$. They produce friction forces that are opposed to the motion. It is necessary to verify that these friction forces are not too relevant with respect to the rated thrust force.

3.6 Optimized design algorithm

A two-step procedure is applied to obtain the optimal design of a series of PM tubular linear actuator. In the first step the integrated model of the motor is utilized for determining the relationships between critical design parameters and machine performance, facilitating the rapid assessment of a large number of potential designs, satisfying magnetic, thermal and mechanical constraints. In the second step, a two-dimensional FEM analysis is adopted to refine the preliminary design, allowing the force ripple to be minimized.

The design optimization can pursue several target, such as the maximum force density, the maximum mover acceleration, etc.. Assuming that the motor will be used in automated industrial machine, then the dynamic performance represents the most meaningful parameter. Thus, the design objective is to select the machine parameters in order to maximize the force density/acceleration and minimize the total force ripple. In the same time, thermal and mechanical constraints have to be satisfied. The thermal limit depends on the insulating material adopted for the stator windings, whereas the mechanical constraints are related to the maximum displacement due to the electromagnetic forces in presence of assembling misalignment.

A. Input parameter and design constraints

The integrated model of the motor can be used to define different design algorithm, each one differs from the others on the parameters chosen as input of the problem.

In particular, input parameters will be used in the design algorithm in different manner on the basis of their meanings. Some inputs define the problem constraints, thus they define one specified value that will be used in the algorithm, while other inputs define a range of

values where one design parameter may vary. Finally, other input parameters set the limit value of certain design parameter, so they represent a condition which determines the discarding of the problem solution not compatible with the aforementioned condition.

The first typology of parameters can be named “fix-constraints”, the second one may be named “range-constraints” while the third one can be called “limit-constraints”. The choice of the input parameters had been done considering the technical issues which concern the realization of the tubular motor with SMCs technology, viz. considering issues of the SMC compaction process. Further, some mechanical constraints had to be fixed in order to use commercial industrial components, thus obtaining a motor with potential low cost.

Among the “fix-constraints”, it is possible to list:

- Number of poles $\rightarrow N_p$;
- Number of slots $\rightarrow N_s$;
- Stator external diameter $\rightarrow d_{ex}$;
- Actuator length $\rightarrow w_{act}$;
- Tooth shoe pole width $\rightarrow w_{ep}$;
- Shoe pole high $\rightarrow h_{ep}$;
- Slider tube width $\rightarrow h_i$;
- Mechanical air-gap length $\rightarrow g$;
- Inner slider bore diameter $\rightarrow d_{sib}$;
- Tooth flux density $\rightarrow B_t$;
- Initial slider eccentricity $\rightarrow v_0$;
- Maximum windings over-temperature $\rightarrow \mathcal{G}_{w-e}$.

These constraints define the motor volume, the main electromagnetic specifications, the maximum windings over-temperature and the initial slider eccentricity due to the assembling misalignment and clearance of the bearings.

The input parameters variable in a reasonable range, defined “range-constraints”, consider the feasibility issues related to SMCs and magnets, and are:

- Maximum and minimum magnet width $\rightarrow w_{m,max}$ and $w_{m,min}$;
- Maximum and minimum inner slider diameter $\rightarrow d_{si,max}$ and $d_{si,min}$;

Finally, the parameter defined as “limit-constraints” are:

- Maximum slider core flux density $\rightarrow B_{p,max}$;
- Maximum slider displacement $\rightarrow y_{max}$.

Keeping the tooth flux density and the slider core flux density limits under the knee of the B-H curve of the magnetic material, iron saturation is avoided. The maximum slider displacement has to be fixed as a small percentage of the mechanical air-gap, let's say 10%.

B. Preliminary design: solution procedure of the integrated model equations

The “fix-constraints” and the “range-constraints” are a problem input, and they can be used to develop the problem solution. For a given set of “fix-constraints” and “limit-constraints”, the following solution procedure can be repeated for each value of w_m and d_{si} included in the “range-constraints”:

- 1) Solving the system of equation formed with (3.1), (3.2), (3.4) and (3.6) then B_m , H_m and B_g can be calculated.
- 2) The value of w_t is obtained using the (3.8), the (3.12) and B_g .
- 3) Substituting w_t in (3.14), then results the value of w_s .
- 4) Using (3.11), (3.15), (3.16), (3.17) and w_t , it is possible to define the values of h_b and h_s .
- 5) Through(3.13) and (3.7), B_{ep} (3.11)and B_p are calculated; B_p is then compared with $B_{ep,max}$ in order to discard/do not discard the current solution.
- 6) The previous result permit to calculate a numerical value for (3.21) and (3.22).
- 7) The solution of the thermal model, as illustrated in subsequent section, permits to calculate P_{cu} .
- 8) Using P_{cu} in (3.23) and substituting the result in (3.24), the slot current is determined. The latter can be used to calculate the thrust force by (3.25).
- 9) Finally, all data are available to calculate (3.44), then (3.43) and finally the slider displacement by (3.42), which is compared with y_{max} in order to discard/do not discard the current solution.

C. Thermal model solution

The substitution of (3.28) and (3.29) in (3.27) define the relation between \mathcal{G}_{f-e} and R_{conv} . Using the latter term and substituting (3.30) in (3.26) yield (3.48).

$$A \mathcal{G}_{f-e}^{5/4} + B \left(\frac{T_{env} + \mathcal{G}_{f-e}}{100} \right)^4 + C = Q_{tot} \quad (3.48)$$

where

$$\begin{cases} A = \left(\frac{5.6 S_V}{\sqrt[4]{h T_{env}}} + \frac{5.6 S_H}{0.5 \sqrt[4]{h T_{env}}} \right) \\ B = \sigma_{rad} (S_V + S_H) \\ C = -\sigma_{rad} \left(\frac{T_{env}}{100} \right)^4 (S_V + S_H) \\ D = \frac{1}{N_s S} \left(\frac{s}{\lambda'} + \frac{2 (w_s - 2s)}{3 \cdot 4 \lambda} \right) \end{cases} \quad (3.49)$$

Equation (3.48) can be solved using Newton-Raphson iterative method to calculate \mathcal{G}_{f-e} . The iterative formula which permits to calculate the frame over-temperature is:

$$\mathcal{G}_{f-e}^{n+1} = \mathcal{G}_{f-e}^n - \frac{f(\mathcal{G}_{f-e}^n)}{f'(\mathcal{G}_{f-e}^n)} \quad (3.50)$$

where

$$\begin{cases} f(\mathcal{G}_{f-e}) = A \mathcal{G}_{f-e}^{5/4} + B \left(\frac{T_{env} + \mathcal{G}_{f-e}}{100} \right)^4 + \frac{\mathcal{G}_{f-e}}{D} + C - \frac{\mathcal{G}_{w-e}}{D} - Q_{tot} \\ f'(\mathcal{G}_{f-e}) = \frac{5}{4} A \mathcal{G}_{f-e}^{1/4} + 4B \left(\frac{T_{env} + \mathcal{G}_{f-e}}{100} \right)^3 \frac{1}{100} + \frac{1}{D} \end{cases} \quad (3.51)$$

D. Finite Element Analysis

The preliminary design obtained with the integrated model of the motor can be further improved using an axis-symmetric finite-element analysis to calculate the flux density distribution in the actuator and the localized saturation in the iron core. The effect of load currents can be evaluated in order to refine the main actuator dimensions, such as tooth width, tooth polar shoe width, etc.. This analysis allows the evaluation of the cogging and end-effect forces, furthermore it permits the correct sizing and the correct positioning of the compensation disks, as shown in Figure 10.

The finite-element analysis can be applied also to the thermal design, in order to determine the temperature distributions in the different part of the actuator, as a consequence of the core losses and winding losses.

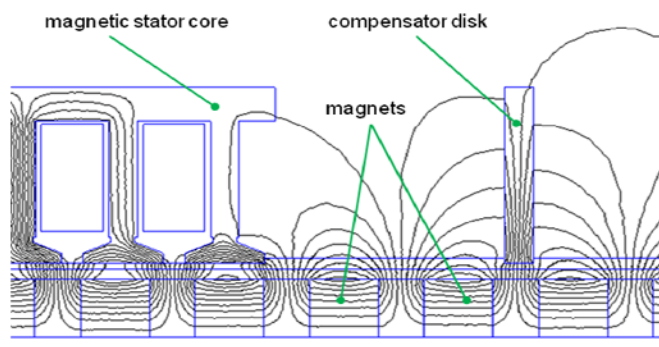


Figure 10-Magnetic field near a compensator disk.

E. Numerical optimization of the number of wire per slot

The dynamic behaviour of the tubular motor strongly influence its servo characteristics, which are very important for automated machine in industrial applications. Thus, the drive performance are limited by both the inverter limits and the motor limit. The former consists in Dc bus voltage, nominal current and overload current, while the latter is the maximum slot current, which define the maximum current before that magnet demagnetization occurs. Thus the number of wires per slot, viz. the number of turns in series per phase, influence the dynamic behaviour of the motor, since the phase parameters and the main motor constants vary with it. It is well known that phase resistance and inductance depend on the square of the number of wires per slot, while the back EMF constant and the force constants depend on the number of wires per slot. Finally, the phase current is inversely proportional to the number of wires per slot for a fixed nominal slot current, which guaranties the invariability of the produced thrust force.

In classic rotary machine the number of wires per slot is sized for a specified voltage and frequency, with constant rotor speed. Tubular linear actuators never operate at constant speed because of its reciprocating motion, thus the number of wires per slot can be considered as a design degree of freedom which can be optimized pursuing a specific target for a given set of inverter and motor limits.

The following constraints are fixed: the DC bus voltage, the nominal current of the inverter, its overload current, the nominal slot current and finally the maximum slot current. The proposed optimization is based on a numerical simulation of the tubular drive with variable number of wires per slot, assuming that the inverter feeds the motor with its full voltage and fixing the mover stroke. The subsequent inertial start up is registered in terms of position, velocity, phase current and slot current. The position transient, together with phase and slot current, is used to select the better number of wires per slot. The selection criterion considers at first the position curve: in first instance, the motor with number of wires per slot which reaches for first the half stroke is considered the better. Then the slot

current transient is analyzed to ensure that its limit is not reached, or at least it lasts for a short period.

The drive model used for this simulation is depicted in Figure 11, where the motor parameters with "*" change their value in concordance with the number of wires per slot and m is the mover mass. The block "current limit" implements the maximum slot current and the overload drive current, thus it limits the phase current in agreement with the aforementioned current constraints. The inverter block considers the DC bus voltage and calculates the v_q voltage considering the amount of v_d voltage necessary to keep the i_d current equal to zero. The calculation required for the latter purpose uses i_q and ω , which enter in the inverter block.

An example of optimization is reported: for a given DC bus voltage, inverter overload current and maximum slot current the transient behaviour of main electric and mechanical characteristics have been registered. The number of wires per slot is measured in per unit (p.u.), and the base value is the number of wires per slot calculated in the same manner of a rotary machine.

Figure 12 shows a typical position transient, for the considered example, a reduction of wires per slot results in a increased dynamic performance, since the half-stroke is quicker reached by motors with slow number of wires per slot. Figure 13 show the phase current in p.u., where the base value is the inverter overload current: the overload constraint never occurs, in fact the maximum phase current value remains under the unity. The current limitations highlighted with a dashed line in Figure 13 is introduced by the slot current limit. Figure 14 depict slot current transient referred to the maximum slot current: the figure highlights with a dashed ellipse the effect of the slot current limit, which it lasts for a period growing with the reduction of the number of wires per slot.

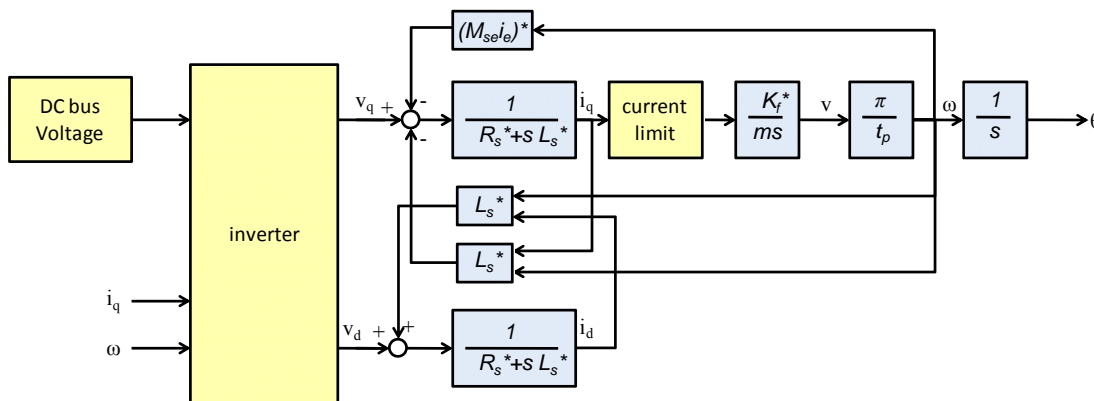


Figure 11-Block diagram of the drive used to optimize the number of wires per slot, paying attention at drive and motor constraints.

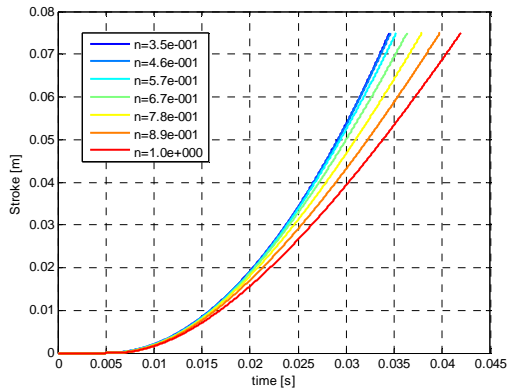


Figure 12-Mover position transient, for a variable number of wires per slot.

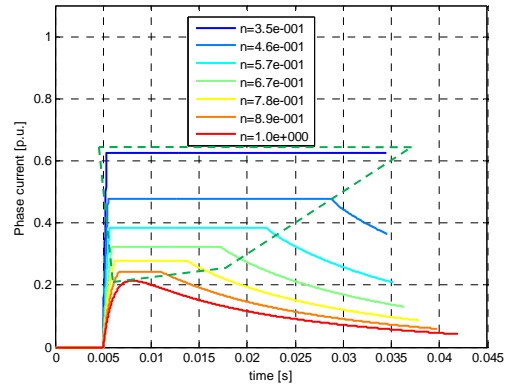


Figure 13-Phase current in p.u. (base value: inverter overload current), for a variable number of wires per slot.

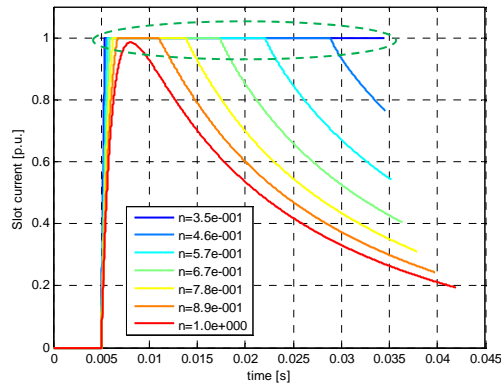


Figure 14-Slot current in p.u. (base value: maximum slot current), for a variable number of wires per slot.

3.7 Conclusion

This chapter presents the mathematical model and an optimal design algorithm used to design of a prototype of permanent magnet actuator, paying attention not only to the electromagnetic issues, but also to the thermal and mechanical constraints. The model allows to manage the relationship between critical design parameters and the machine performance. Further, it permits to develop a large number of optimized motor design quickly, with a precision smaller than $\pm 7\%$. Detail regarding the motor design and their relative experimental results will be presented in next chapter.

CHAPTER

4

Optimized design of a PM tubular linear actuator and experimental results

4.1 Introduction

The design methodology proposed in the previous chapter, which consider electromagnetic, thermal and mechanical issues, will be used to size a three-phase PM tubular linear actuator.

Initially, a preliminary optimized design will be applied in order to analyze the influence of critical design parameters on the machine performance. Hence, a FEM analysis will be used to refine the design and to take into account the end-effect problem. It will follow the optimization of the number of wire per slot.

Finally, experimental results of a prototype of tubular linear actuator will be presented and they will be used to validate the design procedure.

4.2 Definition of the design constraints

The optimized design algorithm can be applied after the definition of the constraints described and listed in Paragraph 3.7 A in Chapter 3.

The first two parameters, N_p and N_s , are crucial for the motor design, indeed they strongly affect the amplitude and the space periodicity of the cogging force. Brushless motors use fractional pitch windings in order to minimize the cogging torque, thus this solution will be adopted to define the number N_p and N_s , since other technical solutions cannot be equally effective for the tubular topology. The choice of $N_p = 8$ and $N_s = 9$ results an optimum compromise for the cogging force issues, since the space periodicity of the cogging force results $1/9$ of the pole pitch. In addition further the equivalent number of slots per phase and per pole is quite high, in particular it is 3.

Other design constraints, such as d_{ex} and w_{act} , define the volume of stator. These two parameters had been chosen in order to obtain a compact motor, since the ratio w_{act}/d_{ex} is 1.6.

Then the stainless steel tube width h_t that contains the magnets and the slider with the SMC poles had been chosen considering the commercial dimensions of such an industrial product. The mechanical air-gap length g represents a crucial parameter, since it strongly influences the performance and the design of the machine. Indeed, the smaller the air-gap is, the highest the thrust force is, but at the same time the radial force and the slider bending become critical. Thus it had been repeated the preliminary optimized design for three different values of g , which are respectively 0.5, 0.75 and 1 mm. The inner bore diameter of the slider d_{sib} has been set in order to guarantee a easy slider feasibility and to improve the motor dynamic feature. The width of the tooth shoe pole w_{ep} had to leave a slot opening larger than the sum between the stainless steel tube width h_t and the mechanical air-gap g , in order to minimize leakage fluxes in slot openings. The thickness of tooth shoe pole has been fixed considering technical issues on the compaction process of the SMCs. The initial slider eccentricity v_0 has been determined considering the typical value of bearing clearance and assuming the presence of mounting misalignment of the slider, fixed at 0.1 mm. The maximum windings over-temperature depends on clearly by the insulation class of the windings, which is class B.

The tooth flux density B_t and the maximum slider core flux density $B_{p,max}$ has been fixed at 1.1 T in order to avoid the saturation of the iron core. Figure 1 shows the B-H curve of Somaloy® 500. It can be seen that the highlighted operational magnetic point is under the knee of the curve.

Then, magnet width limits, viz. $w_{m,max}$ and $w_{m,min}$, have been fixed with the aim to obtain the ratio w_m/t_p within in the range $0.2 \div 0.8$, while the limits of the inner slider diameter $d_{si,max}$ and $d_{si,min}$ have been selected in order to obtain the ratio d_{si}/d_{ex} within in the range $0.16 \div 0.65$. The latter limits are related to the minimum mover diameter and to the minimum slot depth.

Finally, the maximum slider displacement y_{max} of the slider was set to maintain the ratio

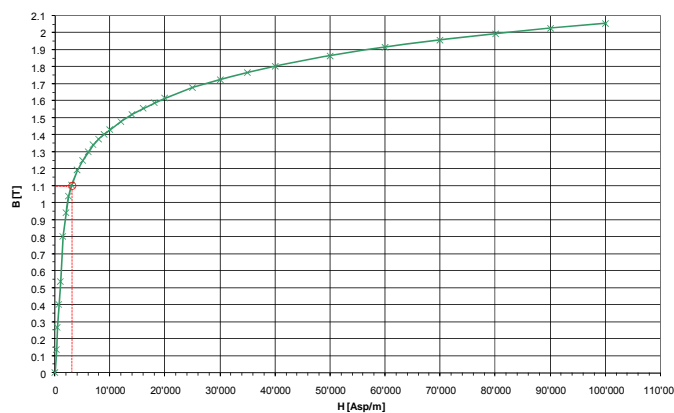


Figure 1-B-H curve of Somaloy® 500, the magnetic operational point is highlighted in the curve.

y_{max}/v_0 under the value 0.1.

4.3 Analysis of the influence of the air-gap length on motor performance

The preliminary design presented in the previous chapter can be used to carry out an analysis of the influence of the air-gap length on the motor performance.

As in the rotating machine, the air-gap length represents a fundamental parameter for the designer, and its value influences both the electromagnetic and the mechanical behaviour. From the magnetic point of view, the designer has to design the machines with thin air-gap, thus higher force density can be achieved. At the same time, from a mechanical point of view, thin air-gap may emphasize the slider bending because of the bending force depends from the initial bearing clearance, on the slider mechanical characteristics and from the square of the air-gap flux density. The bending effect of the slider in a tubular linear motor must not be neglected, since the slider behaves like a thin-beam loaded with distributed force. Thus, a thin air-gap is critical, in fact it can be further reduced by the slider bending and, in some case, creeping between the slider and the stator occurs.

Figure 2 depicts the optimized force density as a function of the ratio d_{si}/d_{ex} , calculated as the ratio between the thrust force computed with the preliminary design equations and the stator volume ($w_{act} \pi d_{ex}^2/4$). It can be observed that the maximum force/volume is achieved for inner slider diameter to external stator diameter included in the range 0.4÷0.5. Further, the mechanical air-gap length influences noticeably the thrust force density.

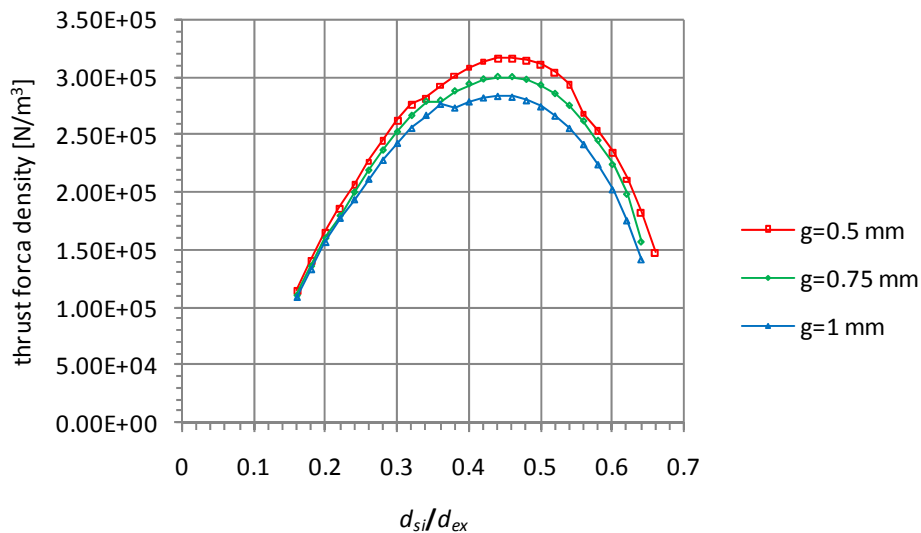


Figure 2-Force-to-stator volume ratio as function of the ratio d_{si}/d_{ex} , computed for three different value of the mechanical air-gap.

Figure 3 and Figure 4 depict respectively the radial force density, which produce the slider bending, and the ratio y_{max}/v_0 , both as a function of the ratio d_{si}/d_{ex} .

Figure 3 shows a rapid growth of the radial force density, indeed its value depends on the square of the air-gap flux density and, for a fixed air-gap length and with growing d_{si}/d_{ex} ratio, its value quickly increases. Considering the equation (3.1), (3.2) and (3.4) in order to obtain the relation between the air-gap flux density B_g and the magnet remanence B_r , and

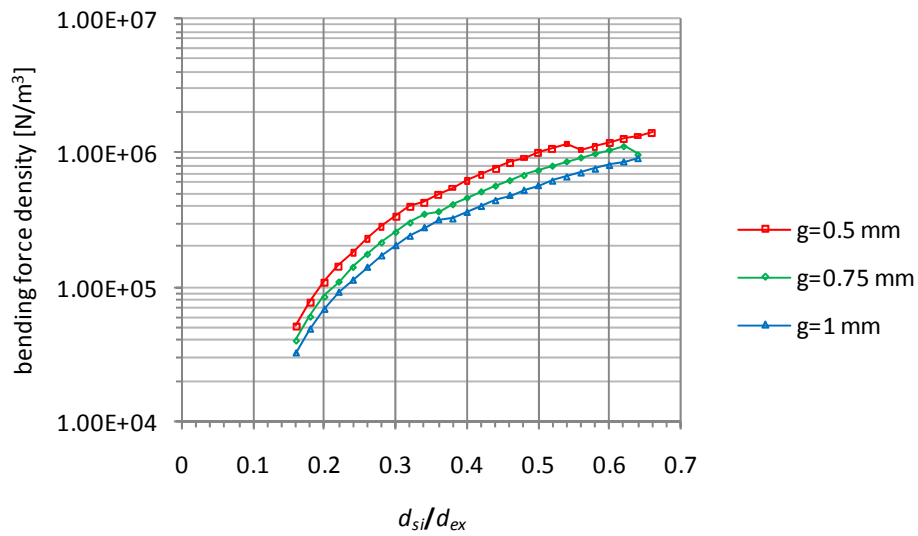


Figure 3-Radial force-to- stator volume ratio as function of the ratio d_{si}/d_{ex} , computed for three different values of the mechanical air-gap.

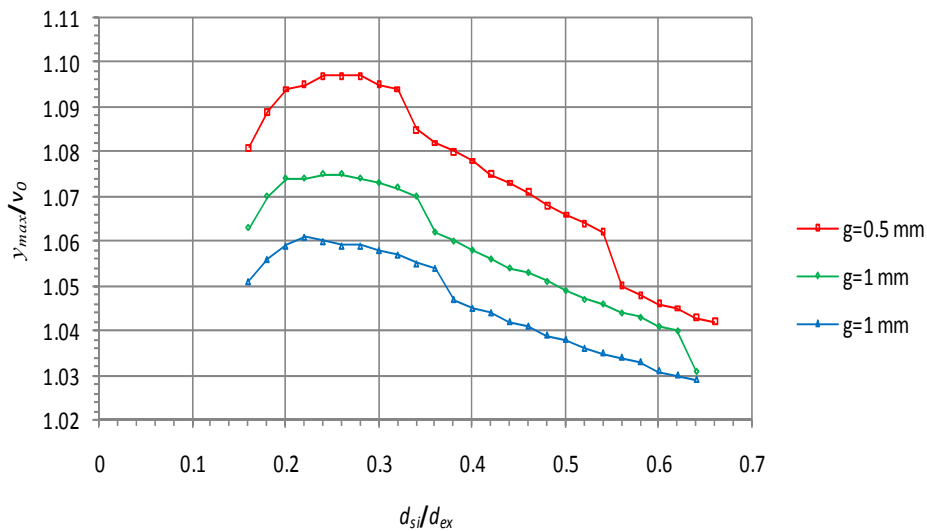


Figure 4-Maximum-to-initial slide displacement ratio as function of the ratio d_{si}/d_{ex} , computed for three different values of the mechanical air-gap.

simplifying the final equation, it results (4.1).

$$B_g = B_r \frac{1}{\left(\frac{2t_p}{d_{si}} + 2 \frac{\delta_0 K_C}{w_m} \right)} \quad (4.1)$$

Equation (4.1) shows that for a given air-gap length g , viz. for a given δ_0 , a growth in the inner slider diameter d_{si} results in an air-gap-flux density increase.

Figure 4 shows the maximum-to-initial slider bending as a function of the ratio d_{si}/d_{ex} , although the increase of the bending force with the ratio d_{si}/d_{ex} is important, the maximum slider displacement decreases with d_{si}/d_{ex} since the moment of inertia of the slider tube with respect to the bending axis increases with the fourth power of d_{si} .

The final analysis of Figure 3 and Figure 4 allows to state that motors with d_{si}/d_{ex} ratio smaller than 0.38÷0.40 exhibit larger slider displacement and lower bending force density than motors with higher d_{si}/d_{ex} ratio. The former have to be preferred than the latter, since large radial force can damage the mechanical sliding system and can strongly reduce the motor reliability.

4.4 Optimized design of a tubular linear actuator

The analysis carried out in the previous paragraph gives some important guidelines for the choice of the motor size among the various proposed by the preliminary design. Thus, it was decided to develop a motor with an air-gap length of 0.5 mm, since the other two solutions do not produce significant advantages in terms of maximum slider displacement and radial force density, while the thrust force density results higher.

A. Preliminary design

The target of the design of the motor is to obtain a tubular actuator suited for automatic industrial application, thus the thrust force do not represent the only choice-parameter, but also the dynamic performance must be considered. Figure 5 depicts respectively the normalized thrust force of the motor (the base value is 35 N) as a function of the d_{si}/d_{ex} ratio, while Figure 6 shows the slider acceleration as a function of the d_{si}/d_{ex} ratio, assuming an inertial payload variable in the range 0÷0.5 kg. The latter Figure shows that an increasing in the additional inertial mass shifts the point of maximum acceleration toward growing values of the d_{si}/d_{ex} ratio.

The d_{si}/d_{ex} ratio range to be selected for the maximum thrust force is 0.4÷0.5, but in this range the dynamic behaviour, measured by the slider acceleration in Figure 6, is very low. The d_{si}/d_{ex} ratio range which maximize the dynamic performance is 0.2÷0.32. Then, a compromise value of the d_{si}/d_{ex} ratio equal to 0.28 was selected. That value is highlighted both in Figure 5 and in Figure 6.

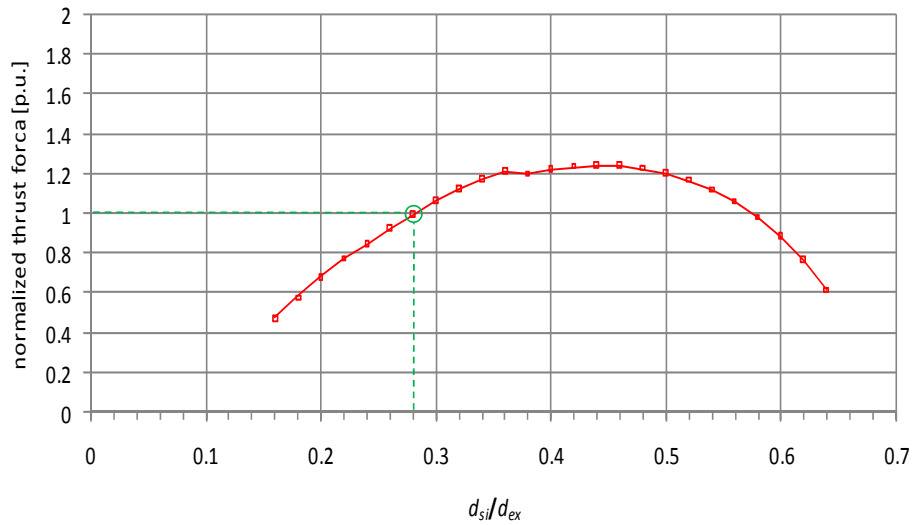


Figure 5-Normalized force as function of the ratio d_{si}/d_{ex} , computed for the mechanical air-gap of 0.5 mm.

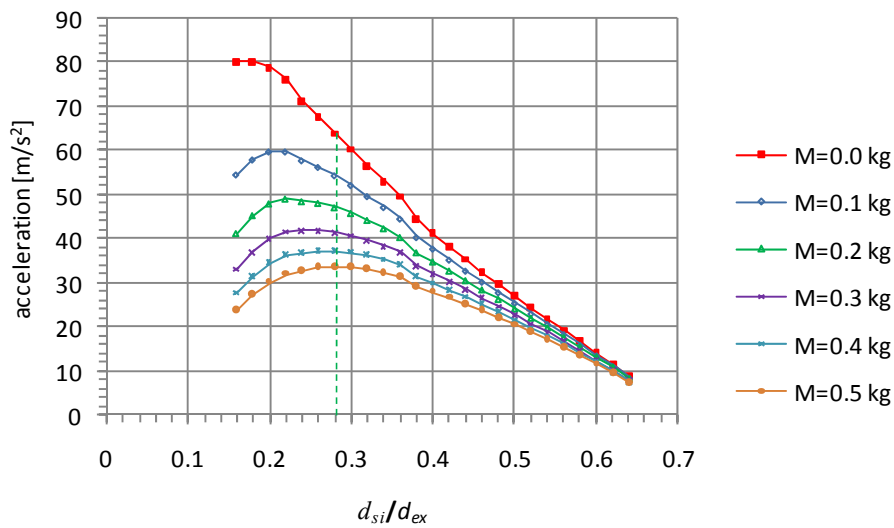


Figure 6-Maximum slider acceleration as function of the ratio d_{si}/d_{ex} , computed for the mechanical air-gap of 0.5 mm and with an additional inertial mass variable in the range $0 \div 0.5$ kg.

B. FEM refining

The main motor dimensions calculated with the preliminary motor design have been used to define a FEM model of the motor, shown in Figure 7. That model was used to verify the preliminary design calculation. Further simulations permitted to analyze the end-effect force disturbance, which has been minimized through the use of a compensator disk. The

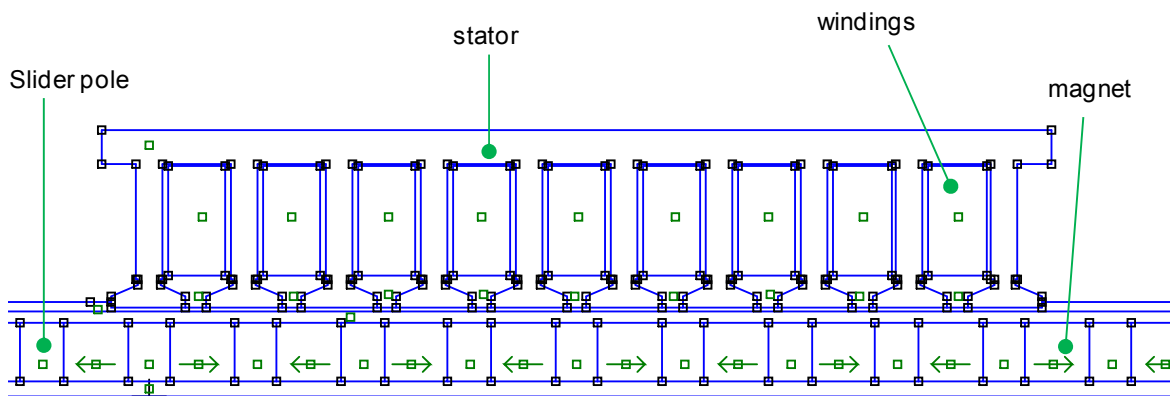


Figure 7-Fem model of the motor sized with the preliminary design.

latter aspect results very important in PM tubular linear actuator, since end effect force ripple deteriorate the slider motion, produces noise, vibrations, etc.

Figure 8 depicts the end-effect force computed with FEM analysis, imposing a null value of the current in the windings, for the motor chosen in the previous paragraph as a function of the slider position; the force is in p.u. and the base value is the motor nominal thrust force of 35 N, while the slider position is referred to the pole pitch.

Figure 9 shows the p.u. reluctance force of one stator disk, computed with FEM model shown in Figure 10, as a function of slider position in p.u.. The comparison between Figure 8 and Figure 9 shows that the force produced by one disk has the same waveform and the same amplitude of the end-effect force of the whole motor. Thus, one disk can be placed in a particular position referred to the stator in order to produce the same force waveform shifted of half space-periodicity, thus the net force with null current in the windings should be minimized. The position of the compensator disk was investigated through a series of

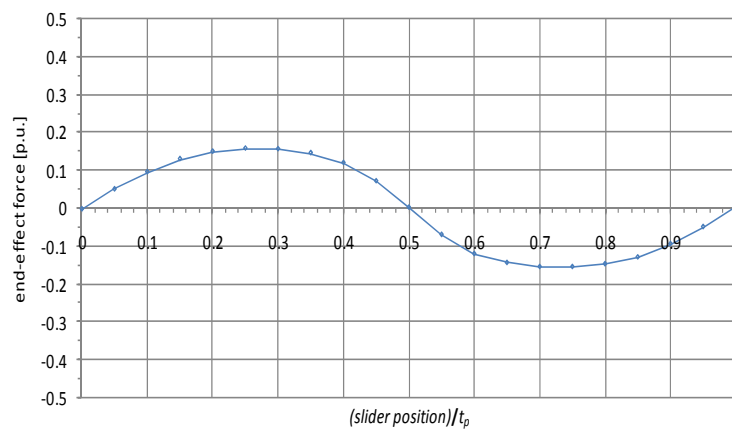


Figure 8-End effect force, normalized to the thrust force, computed by FEM analysis as function of the slider position, expressed in p.u. of the pole pitch t_p .

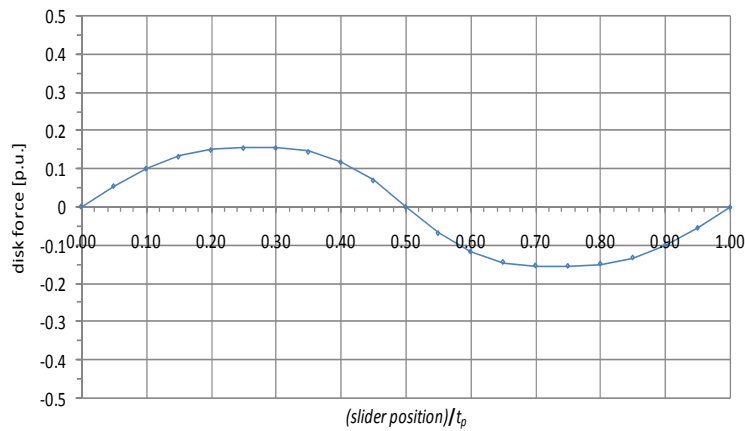


Figure 9-Reluctance force produced by one stator disk, normalized to the thrust force, computed by FEM analysis as function of the slider position, expressed in p.u. of the pole pitch t_p .

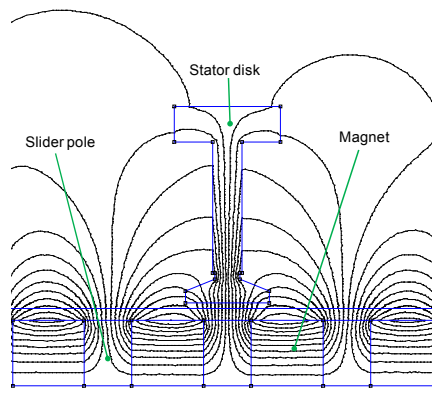


Figure 10-Magnetic flux path of the FEM model of one stator disk.

FEM simulations, where the compensator disk has been shifted in order to determine the optimal position. The final results of this activities are shown in Figure 11, where the optimal compensation of the end effect force results in a very low force ripple.

Finally, it has been calculated the thrust force with a FEM model completed with the compensation system. The sinusoidal stator currents have been imposed to change in synchronism with the slider position, in order to simulate real operative conditions. Figure 12 shows the thrust force produced by the motor: the force ripple is the residual end-effect force, shown in Figure 11, while the circle represents the mean value of the computed thrust force.

C. Optimization of the number of wires per slot

The model proposed in paragraph 3.7 section E has been used to optimize the number of wires per slot in order to fully exploit the tubular linear drive capability. The main results

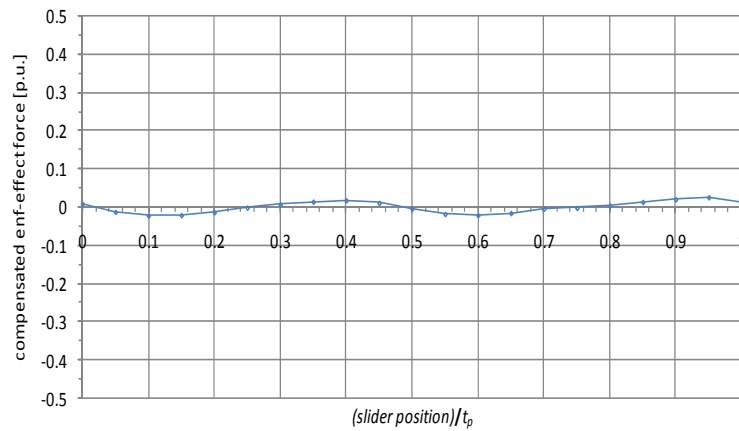


Figure 11-Compensated end-effect force in p.u. as a function of the slider position referred to the pole pitch.

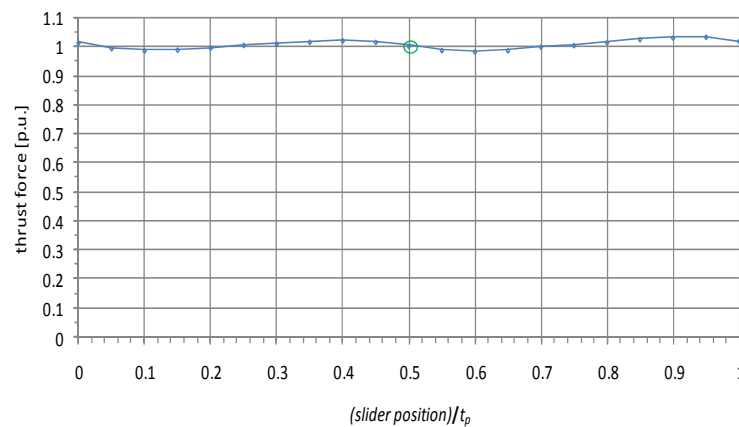


Figure 12-Thrust force values obtained by FEM analysis with sinusoidal stator currents varying synchronously with the position of the slider.

of this optimization are depicted in Figure 13, Figure 14, Figure 15, which show respectively the mover position transient, the phase current transient and the slot current transient.

The base value for the slot and for the phase current are the maximum slot current, which avoids magnet demagnetization, and the maximum phase current of the inverter. The base value for the number of wires per slot is that one calculated in same manner of a rotating machine.

The number of wires which gives better dynamic performance is the smaller one, but this solution results very hazardous, since slot current limit occurs for a long period, as shown in Figure 15. Among the various solution proposed, that one which appears to be a good compromise is pointed out in Figure 13, Figure 14 and Figure 15. Thus, the number of wires per slot has to be reduced by 33% in comparison to the that one calculated in the traditional way.

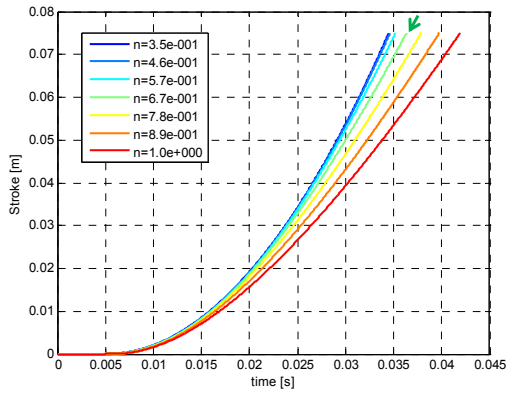


Figure 13-Mover position transient, for a variable number of wires per slot.

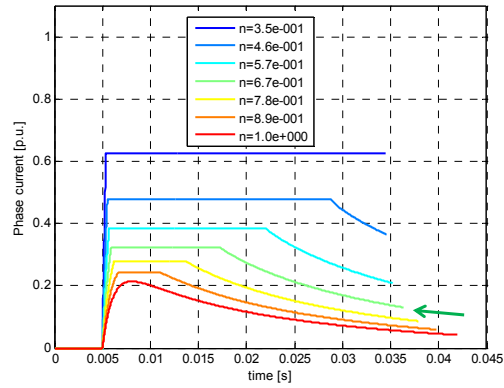


Figure 14-Phase current in p.u. (base value: inverter overload current), for a variable number of wires per slot.

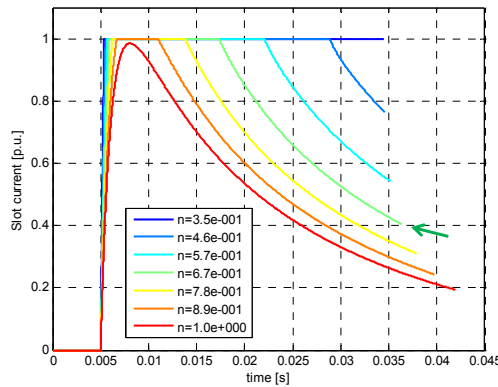


Figure 15-Slot current in p.u. (base value: maximum slot current), for a variable number of wires per slot.

4.5 Experimental results

Figure 16 shows the prototype of a PM tubular motor realized in laboratory in compliance with the design algorithm based on the relationships described in the previous chapter. The stator and the magnetic cylinders of the slider are built in SomaloyTM500 with 0.5% KenolubeTM, compacted to the density of 7.16 g/cm³. The Nd-Fe-B permanent magnets ($B_R=1.1$ T at 20°C) are assembled inside a non-magnetic stainless steel tube.

A. Thrust force

Figure 17 shows the behaviour of the force (normalized with respect to the rated force) produced by the motor with null currents and calculated by means of FEM analysis when the motor is without compensation disks.

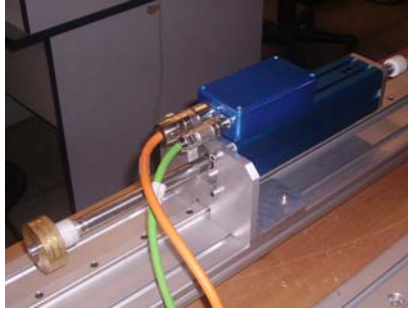


Figure 16-Prototype of tubular motor.

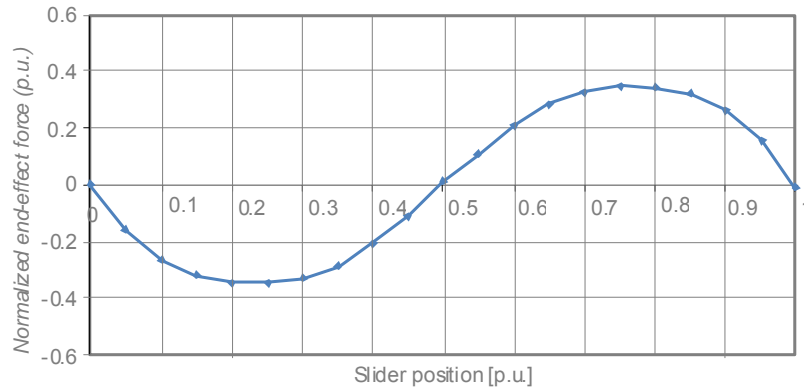


Figure 17-End effect force (normalized with respect the rated thrust force) produced by the motor with null currents, as a function of the slider position (normalized with respect the pole pitch). Behavior of the motor without compensation disks, calculated with FEM analysis

Figure 18 shows the force measured on the prototype. The average force value in Figure 18 is due to the friction of the slider bearings, whereas the superimposed alternative force gives values close to those shown in Figure 17.

The measured values of the force in presence of compensation disks are shown in Figure 19. As can be seen, the compensation disks have practically cancelled the force ripple.

Figure 12 shows the behaviour of the thrust force calculated by means of finite-element analysis, under the assumption that the stator currents vary synchronously with the slider position x according to the following relationships, taking to the field oriented control principles into account.

$$I_k = I_{rated} \sin\left(\pi \frac{x}{t_p} - \frac{2\pi}{3}(k-1)\right) \quad k=1,2,3 \quad (4.2)$$

The average value of the force in Figure 12 corresponds to the rated value. To confirm the analytical results, the following constant currents have been injected in the stator windings:

$$I_2 = I_3 = -\frac{1}{2}I_1 \tag{4.3}$$

where I_1 has the maximum positive value.

Figure 20 shows the force produced by the actuator for different slider positions, apart from the contribution of the friction force shown in Figure 19. It's worth noting that the maximum value of the force measured with constant currents (highlighted by the circle) corresponds to the value of the force calculated with currents synchronized with the slider position, shown in Figure 12. The agreement between experimental and numerical results is satisfactory.

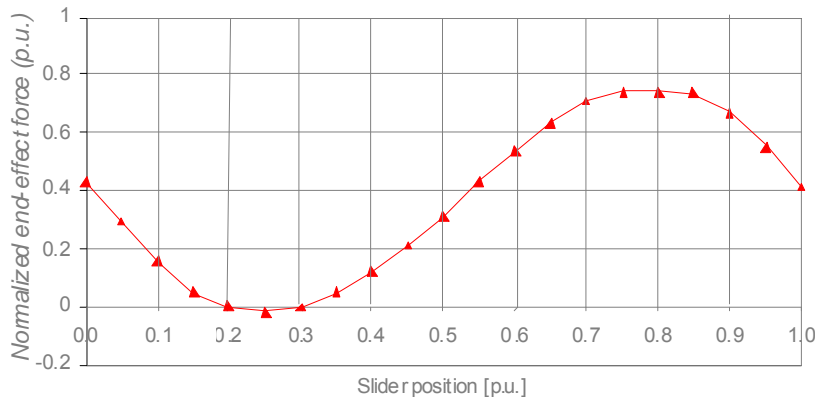


Figure 18-End effect force (normalized with respect the rated thrust force) produced by the motor with null currents, as a function of the slider position (normalized with respect the pole pitch). Behaviour of the motor without compensation disks, measured.

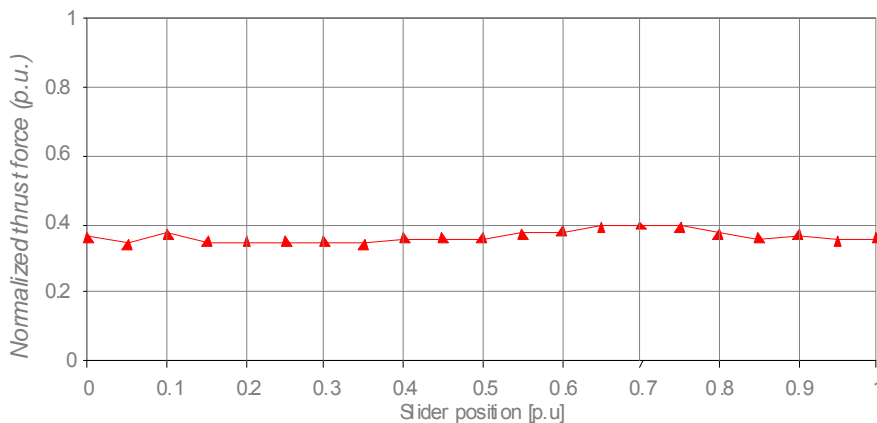


Figure 19-Compensated end-effect force (normalized with respect the rated thrust force) produced by the motor with null currents, as a function of the slider position (normalized with respect the pole pitch), measured.

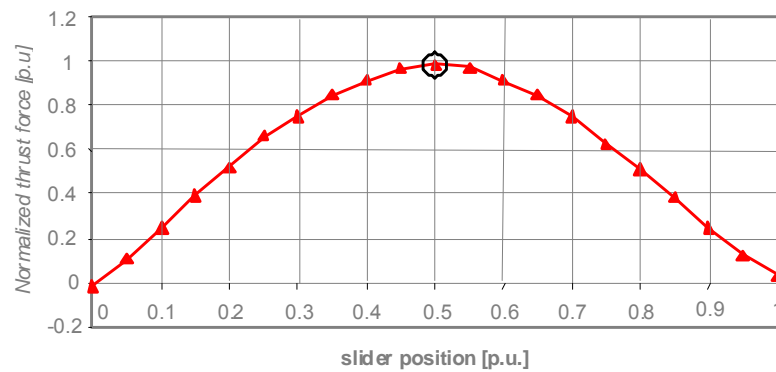


Figure 20-Measured force produced by the actuator with constant values of the stator currents, apart from the contribution of the friction force.

B. Thermal behaviour

A test of thermal characterization in which the power losses are equal to the rated losses has been performed. The calculation of the frame over-temperature by means of the thermal model proposed in the previous chapter leads to values similar to those measured by thermocouples fixed on the external surface of the motor, as shown in Table II.

Finally, the windings-to-environment over-temperature rise was calculated (assuming $\lambda' = 0,2 \text{ Wm}^{-1}\text{K}^{-1}$). Table III compares the numerical results with the measured temperatures. As can be noted, there is a good agreement among all results.

Table II-Frame-to-environment over-temperature.

| | |
|-------------------------------------|---------|
| Value calculated with thermal model | 36.2 °C |
| Average value of the measures | 34.1 °C |

Table III-Average winding-to-environment over-temperature.

| | |
|-------------------------------------|--------|
| Value calculated with thermal model | 46.9°C |
| Measured value | 43.7°C |

4.6 Conclusion

The mathematical model and an optimal design algorithm presented in the previous chapter was used to design a prototype of permanent magnet tubular linear actuator, paying

attention not only to the electromagnetic issues, but also to the thermal and mechanical constraints. The measures carried out on the prototype show a good agreement with the results of the proposed model.

CHAPTER

5

Five-phase dual-motor series-connected drive: simulations and experimental results

5.1 Introduction

Two five-phase tubular linear actuators, having series-connected stator windings of distributed type (number of slot per phase and per pole greater than 1), with an opportune permutation of the phases, can be independently controlled with only one five-phase inverter. This drive structure will be described and analyzed, paying attention on the inverter voltage limit. Then a position control, which is necessary due to the finite length of the slider, will be presented.

Finally, experimental results of the proposed position control of the dual-motor series connected drive will be presented.

5.2 Description of the five-phase dual-motor series-connected drive

The five phase tubular linear motor used for the multi-motor drive has to be designed with special characteristics. Sinusoidal flux density distribution produced by the stator windings is required, then the inverter voltage limit has to be investigated in order to fully exploit the speed-range of the two machines.

A. Motor connections

The independent control of the two five-phase motor is achieved using two independent current space vectors of the five-phase system.

Applying the transformations (2.3) and (2.4) to the five currents of the system i_1, i_2, \dots, i_5 , then three independent space vectors result: \bar{i}_0, \bar{i}_1 and \bar{i}_2 . Relation (2.2) yields the following equation: $\bar{i}_1 = \bar{i}_4^*$ and $\bar{i}_2 = \bar{i}_3^*$. The zero-sequence of the current is null due to the neutral point connection of the phases, while the sequence n°1 and n°3 can be used to control the two five-phase motors connected in series.

The connection scheme with the correct phase transposition can be obtained by the connectivity matrix of Table I in Chapter 2, thus it results the scheme depicted in Figure 1. M_1 and M_2 are the two tubular linear motors, while a, b, c, d, e represent the five windings of each machine.

The proposed phase connection is not the only one which allows the independent control of the five-phase dual-motor drives, since the independent control of the two motors is achieved using each couple of independent current space vectors. All the possible connection schemes can be derived by the combinations of the independent space vectors, which is shown in **Table I**.

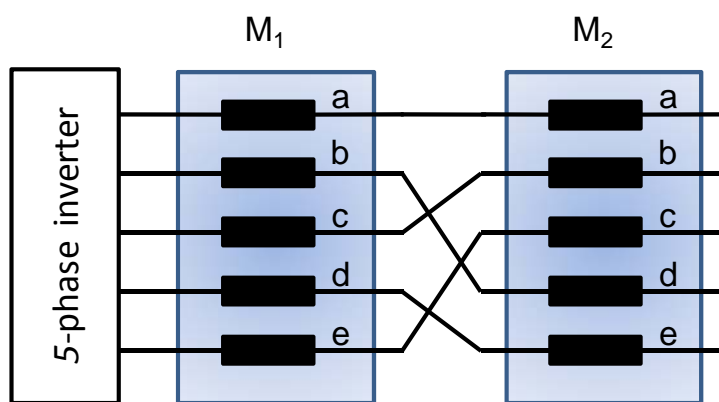


Figure 1-Connection scheme with the phase transposition for the two-motor series connected drive.

Table I-Combinations of independent space vectors for the multi-motor drive.

| M_1 | M_2 |
|-------------|-------------|
| \vec{i}_1 | \vec{i}_2 |
| \vec{i}_1 | \vec{i}_3 |
| \vec{i}_2 | \vec{i}_1 |
| \vec{i}_2 | \vec{i}_4 |
| \vec{i}_3 | \vec{i}_1 |
| \vec{i}_3 | \vec{i}_4 |
| \vec{i}_4 | \vec{i}_2 |
| \vec{i}_4 | \vec{i}_3 |

B. Inverter voltage limit

The inverter voltage limit can be determined using Duty-Cycle Space Vector (DCSV) approach, in fact it permits to define a modulation strategy of a five-phase inverter suited for the problem solution.

Following the well-known carrier-based PWM approach, the DCSV approach directly determines, in each switching period, the switching sequence of each inverter leg. The latter can be obtained comparing a triangular carrier signal with five modulating signals assumed constant in each switching period. The modulating signals are defined by the quantities m_k ($k = 1, 2, \dots, 5$), which represent also the duty-cycles of the five inverter legs.

The modulating signals must satisfy the following constraints:

$$m_k \in [0,1] \quad (k = 1, 2, \dots, 5). \quad (5.1)$$

In order to analyze the modulation strategy, an opportune model is introduced, which is valid considering ideal switches and a switching frequency much higher than the fundamental frequency. Under these assumptions, the higher frequency components of the variables can be neglected, and the input/output quantities are represented by their average values over a switching period T_c .

The generic pole voltage v_{k0} can be written as

$$v_{k0} = V_c m_k, \quad (k = 1, 2, \dots, 5), \quad (5.2)$$

being V_c the voltage of the DC source.

The relationships between the pole voltages v_{k0} and the line-to-neutral load voltages v_{kN} are

$$v_{kN} = v_{k0} - v_{N0}, \quad (k = 1, 2, \dots, 5). \quad (5.3)$$

Note that, owing to the symmetry of the star-connected load, the zero-sequence component of the line-to-neutral load voltages is zero.

Taking (2.3), (5.2) and (5.3) into account, leads to

$$\bar{v}_h = V_c \bar{m}_h, \quad (h = 1, 3), \quad (5.4)$$

$$v_{N0} = \frac{V_c m_0}{2}, \quad (5.5)$$

where the DCSVs \bar{m}_h and the zero-sequence component m_0 of the five-phase inverter are given by

$$\bar{m}_h = \frac{2}{5} \sum_{k=1}^5 m_k \bar{\alpha}^{h(k-1)}, \quad (h = 1, 3), \quad (5.6)$$

$$m_0 = \frac{2}{5} \sum_{k=1}^5 m_k. \quad (5.7)$$

As can be seen from (5.4) and (5.5), the two line-to-neutral load voltages expressed in terms of space vectors are directly proportional to the corresponding DCSVs, whereas the zero-sequence component of the duty-cycle m_0 does not affect the load voltages, but determines the voltage v_{N0} .

A general solution to the modulation problem of the five-phase inverter can be obtained by using (2.6) and (5.4) leading to

$$m_k = \frac{1}{2} m_0 + \frac{1}{V_c} \sum_{h=1,3} \bar{v}_{h,ref} \cdot \bar{\alpha}^{h(k-1)}, \quad (k = 1, 2, \dots, 5). \quad (5.8)$$

Assuming the voltage space vectors $\bar{v}_{h,ref}$ known as reference quantities, then (5.8) allows the calculation of the modulating signals of all the inverter legs in each switching period. The value of m_0 in (5.8) is a degree of freedom which can be utilized to fully exploit the dc voltage, and to optimise some characteristics of the modulation law, such as the number of switch commutations in a switching period and the output voltage spectrum.

The duty-cycles constraints, emphasized in (5.1), introduce complicated limitations on the possible values of $\bar{v}_{1,ref}$ and $\bar{v}_{3,ref}$ in each switching period.

In three-phase inverters this problem involves only the space vector $\bar{v}_{1,ref}$, and it has been already completely solved. In five-phase inverters the analytical solution of this problem represents a very hard task.

The modulation constraints expressed in (5.1) become:

$$m_k - m_i \leq 1, \quad (k = 1, 2, \dots, 5), \quad (i = 1, 2, \dots, 5). \quad (5.9)$$

Substituting (5.8) in (5.9) and taking the relationships (5.4) into account, it is possible to transform the voltage limit problem in the DCSV limit problem, which is independent of V_c , leading to

$$\sum_{h=1,3} \left[\bar{m}_h \cdot \left(\bar{\alpha}^{h(k-1)} - \bar{\alpha}^{h(i-1)} \right) \right] \leq 1, \quad (k = 1, 2, \dots, 5), \quad (i = 1, 2, \dots, 5). \quad (5.10)$$

A more useful expression can be obtained by representing the DCSVs in polar form as follows:

$$\bar{m}_h = |\bar{m}_h| e^{j\beta_h}, \quad (h = 1, 3). \quad (5.11)$$

Taking (5.11) into account, (5.10) can be rewritten as

$$|\bar{m}_1| \sin \left[\beta_1 - (k+i-2) \frac{\pi}{5} \right] \sin \left[(k-i) \frac{\pi}{5} \right] + |\bar{m}_3| \sin \left[\beta_3 - (k+i-2) \frac{3\pi}{5} \right] \sin \left[(k-i) \frac{3\pi}{5} \right] \leq \frac{1}{2}. \quad (5.12)$$

The analysis of (5.12), written for each couple (k, i) (k = 1, 2, ..., 5 and i = 1, 2, ..., 5), allows the determination of the voltage limit in each switching period.

In the case of multi-motor drives, the DCSVs must be completely independent, with arbitrary behaviour, being related to the first spatial harmonics in the two different machines. In general, they can be described as follows:

$$\bar{m}_1 = |\bar{m}_1| e^{j\beta_1}, \quad (5.13)$$

$$\bar{m}_3 = |\bar{m}_3| e^{j\beta_3}. \quad (5.14)$$

It is very interesting to derive the validity domain of $|\bar{m}_1|$ and $|\bar{m}_3|$ regardless of the values of the phase angles β_1 and β_3 .

Taking into account the worst condition for β_1 and β_3 allows (5.12) to be rewritten as

$$|\bar{m}_1| \left| \sin \left[(k-i) \frac{\pi}{5} \right] \right| + |\bar{m}_3| \left| \sin \left[(k-i) \frac{3\pi}{5} \right] \right| \leq \frac{1}{2}, \quad (k = 1, 2, \dots, 5), \quad (i = 1, 2, \dots, 5). \quad (5.15)$$

The five inequalities in (5.15) can be summarized by the two following simultaneous constraints

$$|\bar{m}_1| \sin \left(\frac{\pi}{5} \right) + |\bar{m}_3| \sin \left(\frac{2\pi}{5} \right) \leq \frac{1}{2}, \quad (5.16)$$

$$|\bar{m}_1| \sin\left(\frac{2\pi}{5}\right) + |\bar{m}_3| \sin\left(\frac{\pi}{5}\right) \leq \frac{1}{2}. \quad (5.17)$$

The corresponding validity domain of $|\bar{m}_1|$ and $|\bar{m}_3|$ is represented by the shaded area in Figure 2. This figure can be used by the designer to set the voltage amplitude to size the windings of the five-phase motor. For example, if the dual-motor application require that the two machines work at different speed at the same time, such as the nominal speed for one machine and quasi null speed for the second machine, then $|\bar{m}_i|$ can be selected equal to 0.5; finally the voltage amplitude can be calculated by (5.4).

The windings of the five-phase tubular linear motor have been designed for $|\bar{m}_1| = |\bar{m}_3| = 0.326$, which corresponds to point D in Figure 2, in order to fully exploit their speed-range at the same time.

C. Magnetic design of the five-phase tubular motor

The optimal motor design described in chapter 4 has carried out the optimal dimensions to realize a prototype of PM tubular motor. The stator and the magnetic cylinders of the slider are built in Somaloy[®]500 with 0.5% Kenolube[™], compacted to the density of 7.16 g/cm³, while axial Nd-Fe-B magnets are assembled inside a non-magnetic stainless steel tube, which constitutes the slider. Due to the high cost of the prototype, mainly determined by the mould costs of the stator SMC disks, it has been decided to use one of the main feature of the tubular actuator: the modularity of stator and of the slider. A constrained design of the motor has been carried out, using the same stator disks and the same magnets of the motor designed in chapter 4.

The design aim is to produce sinusoidal-field distribution in the machine air-gap, thus a proper number of slot per phase and per pole have to be chosen. At the same time, a proper ratio between the pole number and the slot number have to be set in order to minimise the

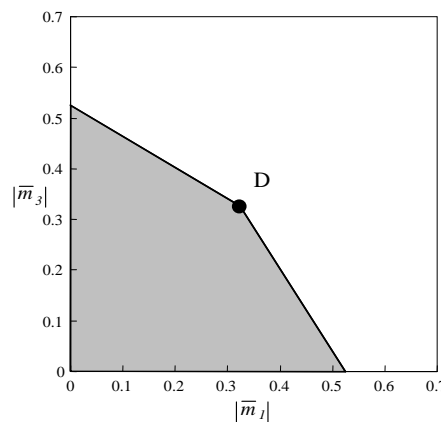


Figure 2-Validity domain of $|\bar{m}_1|$ and $|\bar{m}_3|$ for five-phase dual-motor series connected drive.

cogging force. Further, this ratio should be such that the pole pitch of the five-phase motor results similar to that one of the three-phase prototype of chapter 4. The accomplishment of all of these constraints produces a motor similar to three phase one, considering the magnetic point of view.

If the main geometric parameters of the five phase motor are distinguished through “*” from that ones of the three-phase motor, then the following relations result:

$$N_S t_S = N_P t_P, \quad (5.18)$$

$$N_S^* t_S = N_P^* t_P^*. \quad (5.19)$$

Calculating t_S from (5.18) and substituting it in (5.19) yields(5.20).

$$t_P^* = \frac{N_P}{N_S} \frac{N_S^*}{N_P^*} t_P \quad (5.20)$$

The choice of the $N_P=14$ and $N_S=15$, t_P^*/t_P results in =0.9523, that is a 4.78% of reduction in the pole pitch. Hence, the slider magnetic cylinder width of the five-phase motor decrease by 12% if compared to the slider magnetic cylinder width of the three-phase motor. Further, the proposed numbers of poles and slots result in a winding having an equivalent number of slots per phase and per pole equal to 3, which provides a quasi sinusoidal flux-density distribution in the air-gap of the machine.

FEM analysis has been performed in order to compensate the end effect force, using the same methodologies used for the three-phase motor, and also for analysing the

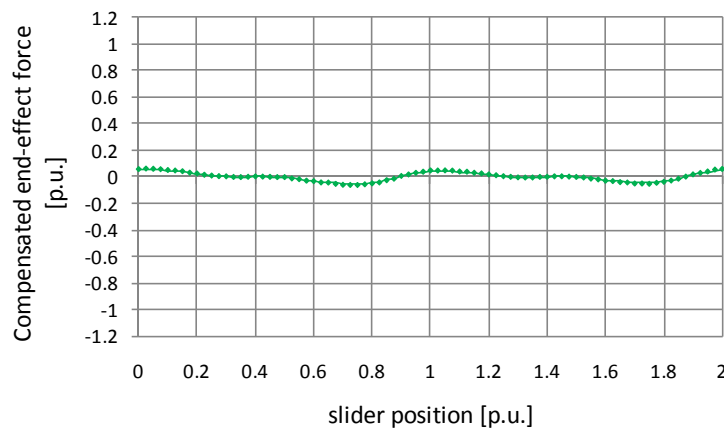


Figure 3-Compensated end-effect force, normalized with the five-phase motor thrust force, as a function of the slider position in p.u..

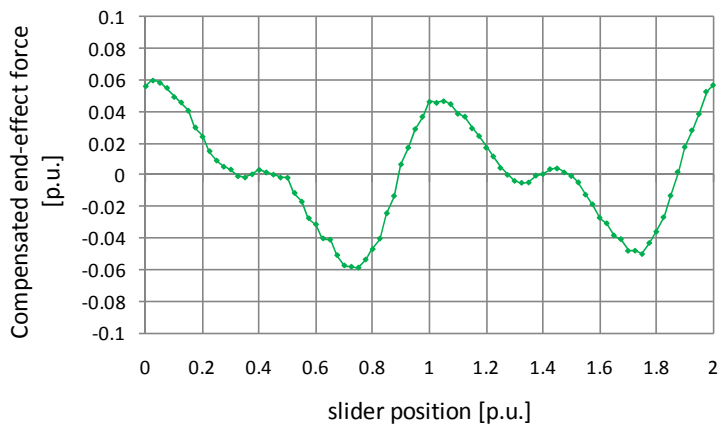


Figure 4-Zoom of the compensated end-effect force, normalized with the five-phase motor thrust force, as a function of the slider position in p.u..

independent control of the motor. Figure 3 shows the compensated end-effect force as a function of the slider position, normalized with the thrust force of the motor. The effectiveness of the proposed compensation method is further confirmed by Figure 4, which is a “zoom” of Figure 3.

Figure 5 depicts the FEM calculation of the compensated thrust force produced by the injection of a constant first current space vector, which corresponds to a set of constant currents i_1, i_2, \dots, i_5 of sequence 1, as a function of the slider position. The thrust force is normalized to the maximum value of its value. The spatial periodicity of the force is $2 t_p$, as in the three phase motor.

Finally, Figure 6 and Figure 7 depict the FEM calculation of the compensated thrust force produced by the injection of a constant third current space vector, which corresponds

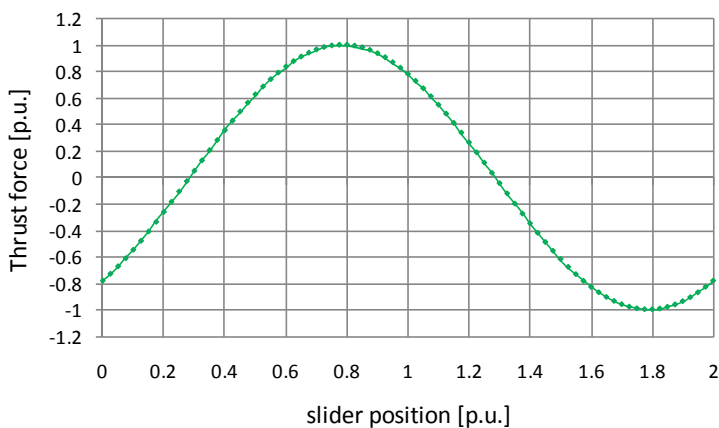


Figure 5-Compensated thrust force produced by the first current space vector, normalized with the five-phase motor thrust force, as a function of the slider position in p.u..

to a set of constant currents i_1, i_2, \dots, i_5 of sequence 3, as a function of the slider position. The spatial periodicity of this force contributions is one third in comparison to that one of the force produced by the fundamental space vector, further its amplitude is similar to the compensated end-effect force. Thus the effect of the third space vector on the force production can be neglected if compared to the force produced by the first current space vector, and independent dual-motor series connected drive can be realized.

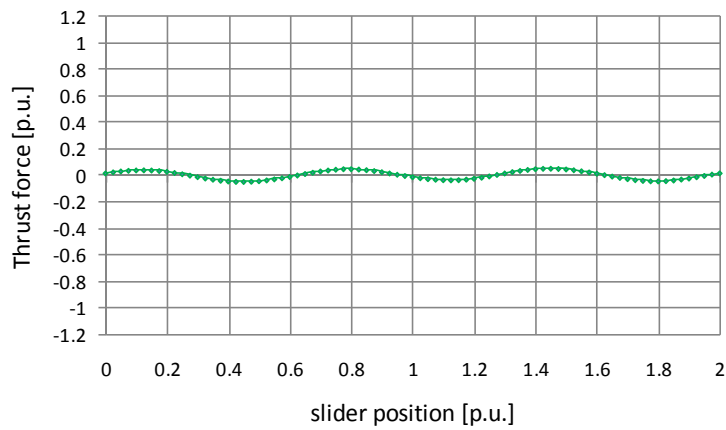


Figure 6-Compensated thrust force produced by the third current space vector, normalized with the five-phase motor thrust force, as a function of the slider position in p.u..

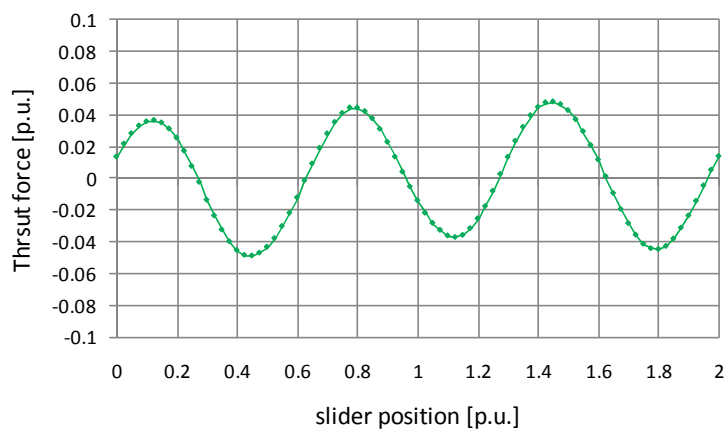


Figure 7-Zoom of the compensated thrust force produced by the third current space vector, normalized with the five-phase motor thrust force, as a function of the slider position in p.u..

D. Control scheme

The fundamental control scheme of the five-phase dual-motor series connected drive is depicted in Figure 8. The motor n°1 (M₁) is controlled by means of the first space vector, while the motor n°2 (M₂) is controlled through the third space vector. The scheme implements a position control for each motor, which will be presented more in details later. The position reference is compared to the slider actual position, thus each motor control generate the corresponding voltage space vector in rotating frame, then they are calculated in the stationary frame by means of each slider measured position. Finally, these references enter in the block of the inverse Clarke transformation, which gives the modulating signals for the inverter legs. Stator currents are measured using LEM sensors, and they are used to calculate the first and the third current space vectors.

Each motor is controlled by the block corresponding “M_M motor control” in Figure 8, in particular each block contains the control scheme shown in Figure 9.

The outer control-loop concerns the position control: the slider position, after a change of measure units, is compared to the actual position and the error passes through a P regulator. Furthermore, a feed-forward regulator, with k gain, acts on the subsequent node, improving the dynamic behaviour of the drive. Then, the speed-regulator elaborates the error signal resulting from the speed-reference, the actual speed and the feed-forward action. Then, the inner control-loop concerns the *q*-component of the current, viz. the rated force, while the *d*-component has a null reference, since the motor operates within its base speed range. Finally, the block for the back-emf compensation provides the voltage space vector in rotating frame.

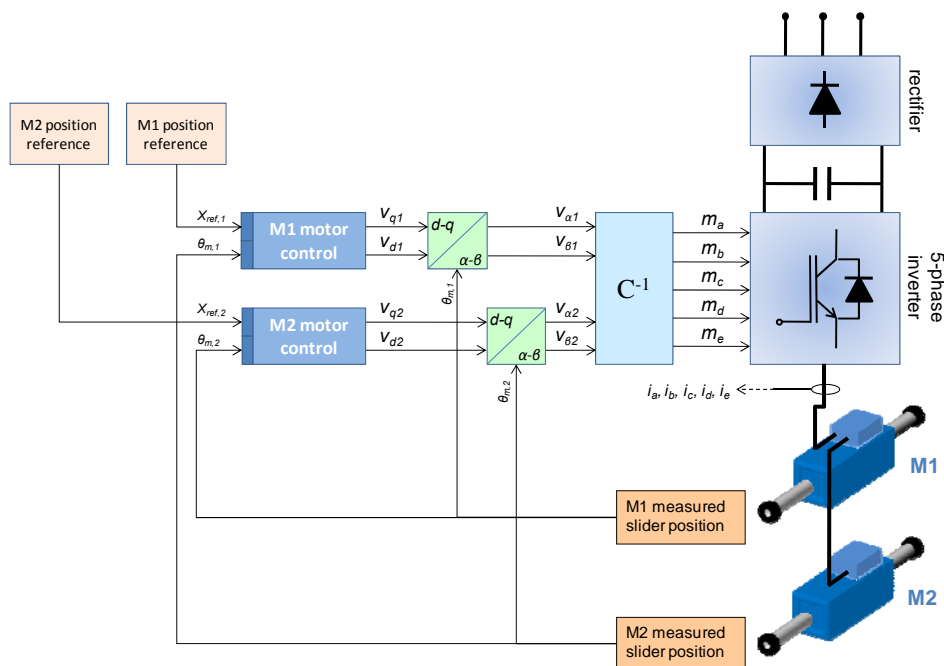


Figure 8-Block diagram of the control scheme.

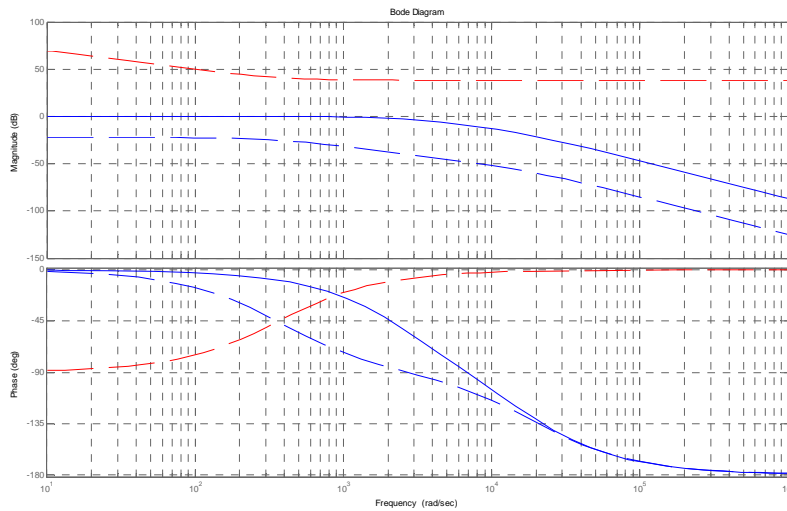


Figure 10-Bode diagram plot of the transfer function from the output of the regulator (a)in the block diagram of Figure 9 to the current i_{q-m} (solid), regulator (red dashed) and compensated system (blue dashed).

5.3 Experimental results

In order to verify the effectiveness of the proposed five-phase dual-motor series connected drive, depicted in Figure 11, some experimental tests have been performed.

The experimental setup consists of a custom-designed five-phase voltage source inverter, shown in Figure 12, feeding a five-phase dual-motor series-connected drive.

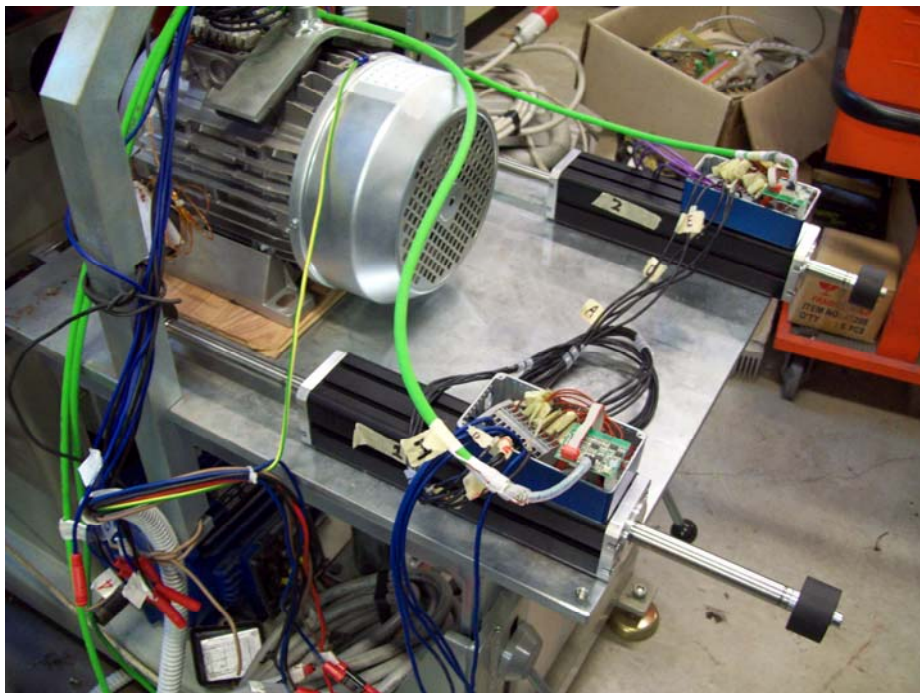


Figure 11-Five-phase dual-motor series connected drive.

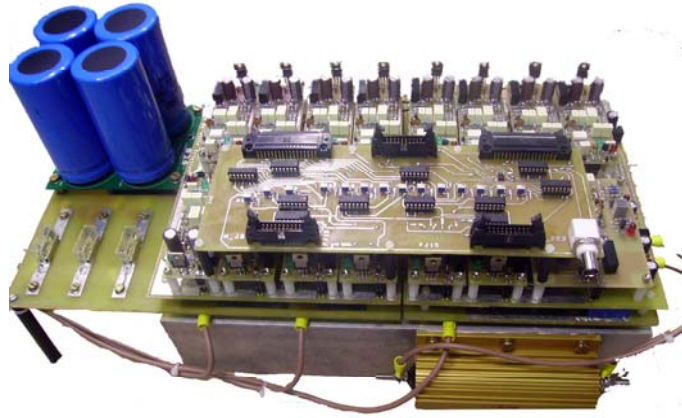
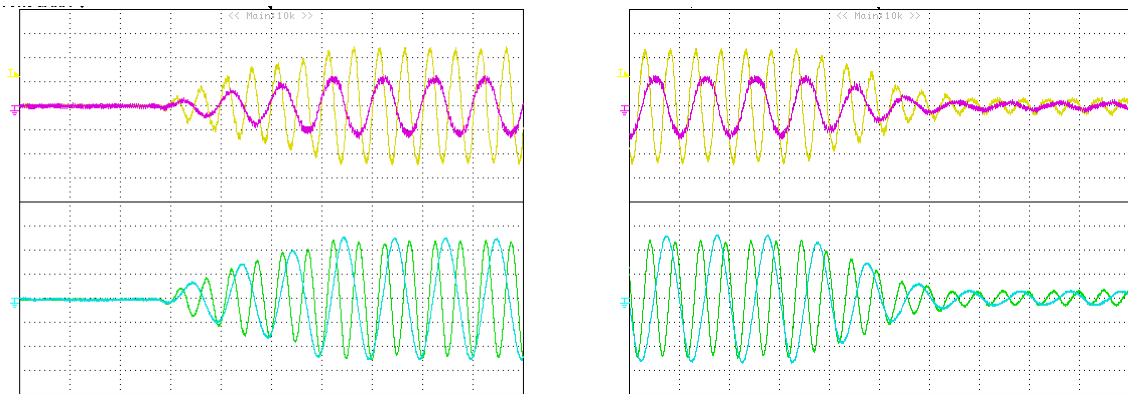


Figure 12-Five-phase inverter.

The control algorithm is implemented in a Digital Signal Processor (DSP) TMS320F2812. The switching period is $100 \mu\text{s}$, corresponding to a switching frequency of 10 kHz.

The position references used to test the multi-motor drive have sinusoidal waveform settable in frequency and amplitude.

A. Start-up test



(a) Experimental test. Behaviour of the multi-motor drive with growing position references. Yellow: M_1 actual speed (5(m/s)/div). Fuxia: M_2 actual speed velocity (5(m/s)/div). Green: M_1 actual position (20cm/div). Ciano: M_2 actual position (20cm/div).

(b) Experimental test. Behaviour of the multi-motor drive with decreasing position references. Yellow: M_1 actual speed (5(m/s)/div). Fuxia: M_2 actual speed (5(m/s)/div). Green: M_1 actual position (20cm/div). Ciano: M_2 actual position (20cm/div).

Figure 13-Start up test: the position references are increased and then decreased in order to test the dynamic behaviour of the control scheme.

B. Position reference variation

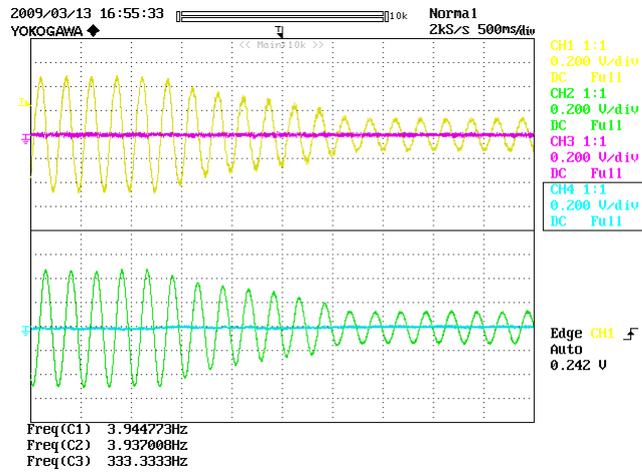
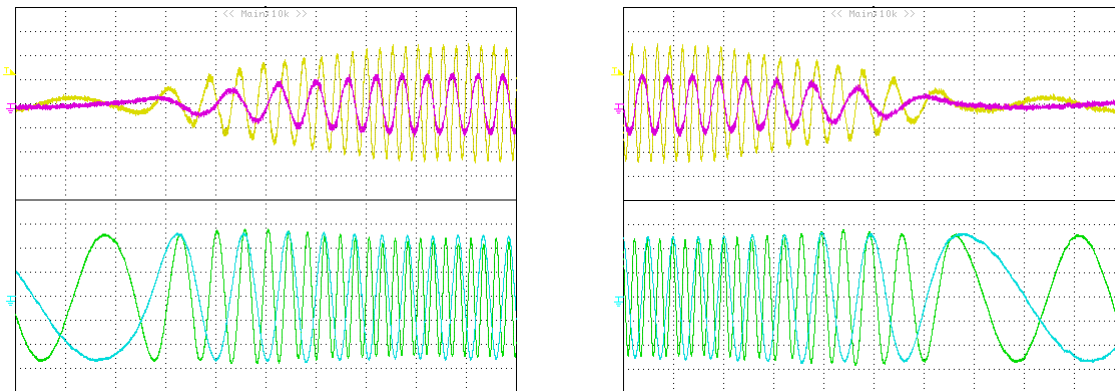


Figure 14-Experimental test. Behaviour of the multi-motor drive with reduction of the M_1 position reference, while M_2 position reference is null. Yellow: M_1 actual speed (5(m/s)/div). Fuxia: M_2 actual speed (5(m/s)/div)). Green: M_1 actual position (20cm/div). Ciano: M_2 actual position (20cm/div).

C. Velocity variation



(a) Experimental test. Behaviour of the multi-motor drive during an acceleration of both motors, for a fixed position amplitude of the sinusoidal position references. Yellow: M_1 actual speed (5(m/s)/div). Fuxia: M_2 actual speed (5(m/s)/div)). Green: M_1 actual position (20cm/div). Ciano: M_2 actual position (20cm/div).

(b) Experimental test. Behaviour of the multi-motor drive during an deceleration of both motors, for a fixed position amplitude of the sinusoidal position references. Yellow: M_1 actual speed (5(m/s)/div). Fuxia: M_2 actual speed (5(m/s)/div)). Green: M_1 actual position (20cm/div). Ciano: M_2 actual position (20cm/div).

Figure 15-Velocity variation test: the position references have a fixed amplitude, while the velocity (frequency) is increased and then decreased.

D. Independent control test

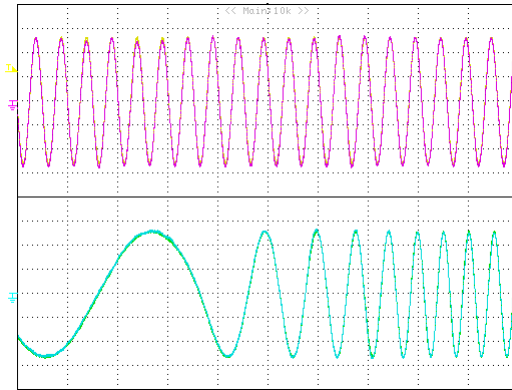


Figure 16-Experimental test. Behaviour of the multi-motor drive with sinusoidal position reference for M_1 , while M_2 position increase its frequency (velocity). Yellow: M_1 position references (20cm/div). Fuxia: M_1 actual position (20cm/div). Green: M_2 position references (20cm/div). Ciano: M_2 actual position (20cm/div).

5.4 Conclusion

The effectiveness of the five-phase dual-motor series connected drive with tubular actuator has been proved, and the consistency of the control scheme has been validated by some experimental tests.

The position control implemented permits to have an independent control of each motor, characterized by a low position error. Further improvement can be achieved using motor with a number of slot per pole and per phase greater than 3.

Conclusions

Linear electric machine are applied in a growing number of industrial applications, since they can be easily integrated in the structure of the application, further enabling the direct drive control. Among the various linear motor topologies, the tubular structure seems to be particularly attractive for industrial purposes due to both its closed form and the inherently absence of attractive force between the stator and the mover. Furthermore, technologic developments in soft and hard magnetic materials have solved the feasibility problems of the iron core and have enhanced the force density of such kind of actuator.

To fully exploit the aforementioned technologic developments and to obtain high performance motors, accurate motor design have to be developed. Thus, the designer has to pay attention not only to the electromagnetic issues, but also to the thermal and mechanical ones.

Nowadays, multiphase drives exhibit excellent feature, especially for the industrial sector. The larger number of degrees of freedom compared with three-phase motor drives enable the implementation of new and promising drive structure, such as the so called multi-motor multiphase drive. Multiphase machines with special design can be connected in series and then independently controlled with a single multiphase inverter, resulting in a more compact structure, with less inverter legs than the three-phase counterpart. Furthermore, the centralized control of such a structure reflects in a high performance drive. The features of the tubular linear actuator and that one of the multiphase drives can be combined in order to obtain automated machine with better characteristics.

In this Thesis work, a mathematical model of the electromagnetic, thermal and of mechanical issues has been developed for PM tubular linear actuators. It has been used as a starting point for an optimal design algorithm definition. The proposed design equations can be used to investigate the behaviour of a the motor as a function of some crucial parameters, such as the air-gap length, the total volume, etc.. The design methodologies described in this Thesis reveal to be effective and precise. Validation was obtained by means of experimental results carried out on a prototype of tubular linear motor.

The control strategies for multi-motor drives have been defined, and the effectiveness of a position control of a five-phase dual-motor series connected drive with tubular actuators has been verified. The independent control of a such a motors has been verified through dynamic tests, which also demonstrate the consistency of the control scheme.

BIBLIOGRAPHY

- [1] E. Masada, "Linear drives for industrial application in Japan – history, existing state and future prospective", Proceedings of LIDIA'95, Japan, pp. 9-12.
- [2] Amitava Basak, "Permanent-magnet DC linear motors", Oxford University Press, 1996, ISBN 0198593929.
- [3] Hamid A. Toliyat, G. B. Kliman, "Handbook of Electric Motors", CRC Press, 2004, ISBN 0824741056.
- [4] I. Boldea, S. A. Nasar, "Linear electric actuators and generators", Cambridge University Press, 1997.
- [5] G.W. McLean, "Review of recent progress in linear motors", IEE Proc. B, 1988, 135, (6), pp. 380-416. E.R.
- [6] Laithwaite, "Linear electric machines - A personal view", Proceedings of the IEEE Volume 63, Issue 2, Feb. 1975 Page(s):250 – 290.
- [7] J.F. Eastham, "Novel synchronous machines: linear and disc", IEE Proc. B, 1990, 31, pp. 49-58.
- [8] I. Boldea, "Linear electromagnetic actuators and their control: a review", EPE-PEMC 2002, Dubrovnik & Cavtat, Croatia, 9-11 Sept. 2002, P.1-P.13.
- [9] J.F. Eastham, F. Profumo, A. Tenconi, G. Gianolio, "Linear drive in industrial application: state of the art and open problems," ICEM 2002, Bruges, Belgium, 25-28 August 2002.
- [10] Marignetti F., Scarano M. "A Linear Tubular Actuator For Robot Arm". INES 2001 - IEEE International 834, Conference on Intelligent Engineering Systems. (vol. 1, pp. 267-272)
- [11] A. K. Buding, "Precision engineering demands for near linear drives in the micrometer and submicrometer range", Proc. I. Mech. Eng., March 1985, pp. 203-213.
- [12] K. Park, E. P. Hong, and K. H. Lee, "Development of a linear motor for compressors of household refrigerators," in Proc. LDIA 2001, Nagano, Japan, 2001, pp. 283–286.
- [13] W. R. Cawthorne et al., "Development of a linear alternator-engine for hybrid electric vehicle applications," IEEE Trans. Veh. Technol., vol. 48, no. 6, pp. 1797–1802, Nov. 1999.
- [14] P. Cancelliere, F. Marignetti, V. Delli Colli, R Di Stefano, M. Scarano, "A Tubular Generator For Marine Energy Direct Drive Applications", IEEE International Electric Machines and Drives Conference, May 15-18, 2005, San Antonio, TX.
- [15] Danson M. Joseph and Willie A. Cronje, "Design and Analysis of a Double-Sided Tubular Linear Synchronous Generator with Particular Application to Wave-Energy Conversion", IEEE PES PowerAfrica 2007 - Conference and Exhibition Johannesburg, South Africa, 16-20 July 2007
- [16] D. Howe, Z.Q. Zhu and R.E. Clark, "Status of linear drives in –Europe", Invited Paper at Linear Drives for Industry Applications (LDIA 2001), Nagano, 2001, pp.468-473.

- [17] V. Di Dio, M. Montana, "State of art of tubular linear induction motor", Electrotechnical Conference, 1996. MELECON '96., 8th Mediterranean, Volume 1, 13-16 May 1996, Page(s):285 - 288 vol.1.
- [18] G. Stumberger, B. Stumberger, D. Dolinar, "Position and current dependent flux linkages, thrust and friction force of linear synchronous reluctance motor", Industry Applications Conference, 2001. Thirty-Sixth IAS Annual Meeting. Conference Record of the 2001 IEEE, Volume 4, 30 Sept.-4 Oct. 2001, Page(s):2310 - 2317 vol.4.
- [19] I. Boldea and S.A. Nasar, "Thrust and normal forces in a segmented-secondary linear reluctance motor," Proc. IEE, vol. 122, no. 9, pp. 922-924, 1975.
- [20] Jang Seok-Myeong, Park Ji-Hoon, You Dae-Joon, Cho Han-Wook, Sung Ho-Kyung, "Design of high speed linear switched reluctance motor", International Conference on Electrical Machines and Systems, 2007. ICEMS. 8-11 Oct. 2007, Page(s):1668 – 1671.
- [21] Lee Byeong-Seok, Bae Han-Kyung, P. Vijayraghavan, R. Krishnan, "Design of a linear switched reluctance machine", IEEE Transactions on Industry Applications, Volume 36, Issue 6, Nov.-Dec. 2000, Page(s):1571 – 1580.
- [22] N.S. Lobo, Hong Sun Lim, R. Krishnan, "Comparison of Linear Switched Reluctance Machines for Vertical Propulsion Application: Analysis, Design, and Experimental Correlation", IEEE Transactions on Industry Applications, Volume 44, Issue 4, July-Aug. 2008, Page(s):1134 – 1142.
- [23] T. Ishii, "Elevators for skyscrapers", IEEE Spectr., vol. 31, no. 9, pp. 42-46, Sep. 1994.
- [24] Sang Heon Lee, Yoon Su Baek, "Contact-free switched reluctance linear actuator for precision stage", IEEE Transactions on Magnetics, Volume 40, Issue 4, Part 2, July 2004, Page(s):3075 – 3077.
- [25] Husain, "Minimization of torque ripple in SRM drives", IEEE Trans. Ind. Electron., vol. 49, pp. 28-39, Feb. 2002.
- [26] N. Bianchi, S. Bolognani, J. Corda, "Tubular linear motors: a comparison of brushless PM and SR motors", International Conference on Power Electronics, Machines and Drives, 2002. (Conf. Publ. No. 487)4-7 June 2002, Page(s):626 – 631.
- [27] J. Corda, "Cylindrical linear stepper motor", IEE Colloquium on Stepper Motors and Their Control, 25 Jan 1994, Page(s):8/1 - 8/4.
- [28] D. Casadei, C. Rossi, G. Serra, A. Tani, "Optimal design of a tubular hybrid stepping motor under volumetric constraints", Proc. of SPEEDAM 2004, Capri (Italy), June 16-18, 2004, pp. 857-863.
- [29] D.J. de Groot, C.J. Heuvelman, "Tubular linear induction motor for use as a servo actuator", Electric Power Applications, IEE Proceedings B, Volume 137, Issue 4, July 1990, Page(s):273 – 280.
- [30] J.F. Eastham, R. Akmesse, H. C. Lai, "Optimum design of brushless tubular linear machines", IEEE Trans. on Magnetics, Vol. 26, No. 5, September 1990, pp. 2547-2549.
- [31] J. Wang, G.W. Jewell, d. Howe, "Design optimisation and comparison of tubular permanent machine topologies," IEE Proc. Electr. Power Appl. , Vol. 148, No. 5, Sept. 2001, pp. 456- 464.

- [32] L. El Amraoui, F. Gillon, A. Castelain, P. Brochet, M. Benrejeb, "Experimental validation of a linear tubular actuator design," ICEM 2002, Bruges, Belgium, 25-28 August 2002.
- [33] P.J. Hor, Z.Q. Zhu, D. Howe, J. Rees-Jones, "Minimization of cogging force in a linear permanent magnet motor", IEEE Transactions on Magnetics, Volume 34, Issue 5, Part 1, Sept. 1998, Page(s):3544 – 3547.
- [34] C.A. Borghi, D. Casadei, A. Cristofolini, M. Fabbri, G. Serra, "Application of a multi-objective minimization technique for reducing the torque ripple in permanent magnet motors", IEEE Trans. on Magnetics, Vol. 35, No. 5, September 1999, pp. 4238-4246.
- [35] T. Yoshimura, H.J.Kim, M. Wanata, M. Torii, D. Ebihara, "Study on the reduction of detent force of permanent magnet linear synchronous motor", IEEE Trans. on Magn., vol. 31, no. 6, pp. 3728-3730, Nov. 1995.
- [36] Z.Q. Zhu, X.P. Xia, D. Howe, P.H. Mellor, "Reduction of cogging force in slotless linear permanent magnet motors," IEE Proc- Elecfr. Power Appl., vol. 144, no. 4, pp. 277-282, July 1997.
- [37] J.Y. Hung, Z. Ding, "Design of currents to reduce torque ripple in brushless permanent magnet motors", Electric Power Applications, IEE Proceedings B, Volume 140, Issue 4, July 1993, Page(s):260 – 266.
- [38] A. Canova, G. Gruosso, M. Otella, M. Repetto, N. Schofield, "Soft magnetic composites for tubular linear actuators," ICEM 2002, Bruges, Belgium, 25-28 August 2002.
- [39] J. Wang, G.W. Jewell, d. Howe, "Design optimisation and comparison of tubular permanent machine topologies", IEE Proc. Electr. Power Appl. , Vol. 148, No. 5, Sept. 2001, pp. 456- 464.
- [40] Lars Hultman, Zhou Ye, "Soft Magnetic Composites - Properties and Applications", PM²TEC 2002 in Orlando, USA.
- [41] Lars Hultman, Mats Persson and Per Engdahl, "Soft Magnetic Composites for Advanced Machine Design", PMAAsia2005, in Shanghai, China.
- [42] Lars O. Hultman (Höganäs AB), Alan G. Jack (University of Newcastle upon Tyne, United Kingdom), "Soft Magnetic Composites - Motor Design Issues and Applications", PM²TEC 2004, in Chicago, USA.
- [43] Jiabin Wang, D. Howe, "Influence of soft magnetic materials on the design and performance of tubular permanent magnet machines", IEEE Transactions on Magnetics, Volume 41, Issue 10, Oct. 2005, Page(s):4057 – 4059.
- [44] E. Levi, R. Bojoi, F. Profumo, H. A. Toliyat, S. Williamson, "Multiphase induction motor driver - a technology status review", in IEE Electr. Power Appl., 2007, Vol. 4, No. 1, pp.489-516.
- [45] E. Levi, "Multiphase Electric Machines for Variable-Speed Applications", IEEE Transactions on Industrial Electronics, Volume 55, Issue 5, May 2008, Page(s):1893 – 1909.
- [46] G. Grandi, G. Serra, A. Tani, "General analysis of multi-phase systems based on space vector approach", in Proc. of 12th Power Electronics and Motion Control Conference (EPE-PEMC), 2006, CD-ROM paper T2-409.

- [47] D. Casadei, F. Milanese, G. Serra, A. Tani, L. Zarri, "Space vector modulation based on a multidimensional approach for multiphase inverters with an odd number of phases", Power Electronics Specialists Conference, PESC 2008. IEEE, 15-19 June 2008, Page(s):1351 - 1357.
- [48] Grandi, G.; Serra, G.; Tani, A., "General Analysis of Multi-Phase Systems Based on Space Vector Approach", Power Electronics and Motion Control Conference, EPE-PEMC 2006. 12th International, Volume 3, Aug. 30 2006-Sept. 1 2006, Page(s):834 – 840.
- [49] M. Benatmane, T. McCoy, T. Dalton, and T. L. Cooper, "Electric power generation and propulsion motor development for US Navy surface ships", in Proc. All Electric Ship: Developing Benefits for Maritime Applications Conf., London, U. K., Sep. 1998, pp. 89–94.
- [50] P. T. Norton, P. E. Thompson, "The naval electric ship of today and tomorrow", in Proc. 3rd All Electric Ship Symp., Paris, France, Oct. 2000, pp. 80–86.
- [51] E. Levi, "Multiphase Electric Machines for Variable-Speed Applications", IEEE Transactions on Industrial Electronics, Volume 55, Issue 5, May 2008, Page(s): 1893 – 1909.
- [52] L. Parsa, "On advantages of multi-phase machines", in Proc. of Annual Conference of the IEEE Industrial Electronics Society (IECON), 2005, pp. 1574-1579.
- [53] S. Williamson and S. Smith, "Pulsating torques and losses in multiphase induction machines", in Proc. IEEE Ind. Appl. Soc. Annu. Meeting IAS'01, Chicago, IL, 2001.
- [54] H.A. Toliyat, T.A. Lipo, J.C. White, "Analysis of a concentrated winding induction machine for adjustable speed drive applications. I. Motor analysis", IEEE Transactions on Energy Conversion, Vol. 6, Issue 4, Dec. 1991, pp. 679-683.
- [55] H.A. Toliyat, T.A. Lipo, J.C. White, "Analysis of a concentrated winding induction machine for adjustable speed drive applications. II. Motor design and performance", IEEE Transactions on Energy Conversion, Vol. 6, Issue 4, Dec. 1991, pp. 684-692.
- [56] E. Levi, M. Jones, S. N. Vukosavic, and H. A. Toliyat, "A novel concept of a multiphase, multimotor vector controlled drive system supplied from a single voltage source inverter", IEEE Trans. Power Electron., vol. 19, no. 2, pp. 320–335, Mar. 2004.
- [57] L. Parsa, H.A. Toliyat, "Five-phase permanent-magnet motor drives", IEEE Trans. on Industry Applicat., vol. 41, no. 1, 2005, pp. 30-37.
- [58] H. Xu, H.A. Toliyat, L.J.Petersen, "Five-phase induction motor drives with DSP-based control system", IEEE Trans. on Power Electron, vol. 17, no. 4, 2002, pp. 524-533.
- [59] Y. Zhao, T.A. Lipo, "Space Vector PWM Control of Dual Three-Phase Induction Machine Using Vector Space Decomposition", IEEE Transactions on Industry Applications, Vol. 31, Issue 5, Sept./Oct. 1995, pp.1100–1009.
- [60] S. Lu, K. Corzine, "Direct Torque Control of Five-Phase Induction Motor Using Space Vector Modulation with Harmonics Elimination and Optimal Switching Sequence", Applied Power Electronics Conference and Exposition, 2006, March 19, 2006, pp. 195-201.

- [61] L. Parsa, N. Kim, H.A. Toliyat, "Field Weakening Operation of High Torque Density Five-Phase Permanent Magnet Motor Drives", IEEE International Conference on Electric Machines and Drives, May 15, 2005, pp. 1507–1512.
- [62] C.B. Jacobina, I.S. Freitas, T.M. Oliveira, E.R.C. da Silva, A.M.N. Lima, "Fault tolerant control of five-phase AC motor drive", Power Electronics Specialists Conference, 2004, Vol. 5, 20-25 June 2004, pp. 3486-3492.
- [63] H.A. Toliyat, "Analysis and simulation of five-phase variable-speed induction motor drives under asymmetrical connections", IEEE Transactions on Power Electronics, Vol. 13, Issue 4, July 1998, pp. 748–756.
- [64] Y. Zhao, T.A. Lipo, "Modelling and Control of a Multi-Phase Induction Machine with Structural Unbalance, Part. I, Machine Modelling and Multi-Dimensional Current Regulation", IEEE Transactions on Energy Conversion, Vol. 11, Issue 3, Sept. 1996, pp. 570–577.
- [65] Y. Zhao, T.A. Lipo, "Modelling and Control of a Multi-Phase Induction Machine with Structural Unbalance, Part. II, Field-Oriented Control and Experimental Verification", IEEE Transactions on Energy Conversion, Vol. 11, Issue 3, Sept. 1996, pp. 578–584.
- [66] M. Benatmane and T. McCoy, "Development of a 19 MW PWM converter for U.S. Navy surface ships", Proc. Int. Conf. on Electric Ship ELECSHIP, Istanbul, Turkey, 1998, pp. 109–113.
- [67] C.L. Ferreira and R.W.G. Bucknall, "Modelling and real-time simulation of an advanced marine full-electrical propulsion system", Proc. IEE Power Electronics, Machines and Drives Conf. PEMD, Edinburgh, Scotland, 2004, pp. 574–579.
- [68] S. Mantero, E. De Paola, and G. Marina, "An optimised control strategy for double star motors configuration in redundancy operation mode", Proc. European Power Electronics and Applications Conf. EPE. Lausanne, Switzerland, 1999, CD-ROM paper no. 013.
- [69] S. Mantero, A. Monti, and S. Spreafico, "DC-bus voltage control for double star asynchronous fed drive under fault conditions", Proc. IEEE Power Electronics Specialists Conf. PESC, Galway, Ireland, 2000, pp. 533–538.
- [70] A.N. Golubev, and V. Ignatenko, "Anomalous operation of multiphase asynchronous electric drive", Russ. Electr. Eng., 2001, 72, (10), pp. 22–28.
- [71] A. Iqbal, S.N. Vukosavic, E. Levi, M. Jones, H.A. Toliyat, "Dynamics of a series-connected two-motor five-phase drive system with a single-inverter supply", in Proc. of IEEE Ind. Appl. Soc. Annual Meeting (IAS), 2005, pp. 1081-1088.
- [72] A. Iqbal, E. Levi, M. Jones, S.N. Vukosavic, "A PWM scheme for a five-phase VSI supplying a five-phase two-motor drive", in Proc. of Annual Conference of the IEEE Industrial Electronics Society (IECON), 2006, pp. 2575-2580.
- [73] E. Levi, M. Jones, S.N. Vukosavic, "A Series-Connected Two-Motor Six-Phase Drive With Induction and Permanent Magnet Machines", IEEE Transactions on Energy Conversion, Vol. 21, Issue 1, March 2006, pp. 121 – 129.

- [74] D. Casadei, G. Serra, A. Tani, L. Zarri, "General inverter modulation strategy for multi-phase motor drives", Proc. of ISIE, Vigo (Spain), CD-ROM, pp.1131-1137, June 4-7, 2007.
- [75] E. Levi, M. Jones, S.N. Vukosavic, H.A. Toliyat, "Operating principles of a novel multiphase multimotor vector-controlled drive", IEEE Transaction on Energy Conversion, Volume 19, Issue 3, Sept. 2004, Page(s):508 – 517.
- [76] M. Jones, S. N. Vukosavic, and E. Levi, "Independent vector control of a six-phase series-connected two-motor drive," in Proc. 2nd IEE Int. Conf. Power Electronics, Machines and Drives PEMD, Edinburgh, U.K., 2004, pp. 879–884.
- [77] M. Jones, E. Levi, and A. Iqbal, "A five-phase series-connected two-motor drive with current control in the rotating reference frame," in Proc. IEEE Power Elec. Spec. Conf. (PESC), Aachen, Germany, 2004, pp. 3278–3284.
- [78] N. Bianchi, "Analytical field computation of a tubular permanent-magnet linear motor", IEEE Transactions on Magnetics, Volume 36, Issue 5, Part 2, Sept 2000, Page(s):3798 – 3801.
- [79] J. Wang, D. Howe, G.W. Jewell, "Analysis and design optimization of an improved axially magnetized tubular permanent-magnet machine", IEEE Transaction on Energy Conversion., Volume 19, Issue 2, June 2004, Page(s):289 - 295 Art n°8.
- [80] N. Bianchi, S. Bolognani, F. Tonel, "Design criteria of a tubular linear IPM motor", Electric Machines and Drives Conference, 2001. IEMDC 2001. IEEE International 2001, Page(s):1 – 7.
- [81] N. Bianchi, S. Bolognani, D. Cortese, F. Tonel, "Tubular linear permanent magnet motors: an overall comparison", IEEE Transactions on Industry Applications, Volume 39, Issue 2, March-April 2003, Page(s):466 – 475.
- [82] R. E. Clark, D. S. Smith, P. H. Mellor, and D. Howe, "Design optimization of moving-magnet actuators for reciprocating electro-mechanical systems", IEEE Trans. Magn., vol. 31, pp. 3746–3748, Nov. 1995. Art n°8.
- [83] T. Mizuno and H. Yamada, "Magnetic circuit analysis of a linear synchronous motor with permanent magnets", IEEE Trans. Magn., vol. 28, pp. 3027–3029, Sept. 1992. Art n°8.
- [84] F. Marignetti, P. Cancelliere, M. Scarano, "Analytical formulation of the no-load magnetic field in IPM tubular machines with translator eccentricity", IEEE Industrial Electronics, IECON 2006 - 32nd Annual Conference on, 6-10 Nov. 2006, Page(s):829 – 835.
- [85] F. Marignetti, P. Cancelliere, V. Delli Colli, R. Di Stefano, M. Scarano, "Analytical Formulation of Radial Magnetic Forces in PM Linear Tubular Machines with Translator Eccentricity", Industry Applications Conference, 2007. 42nd IAS Annual Meeting. Conference Record of the 2007, IEEE 23-27 Sept. 2007, Page(s):530 – 536.